Research Square

Preprints are preliminary reports that have not undergone peer review.
They should not be considered conclusive, used to inform clinical practice,
or referenced by the media as validated information.

Comparative assessment of potentially toxic elements geochemistry in various dusts in Southwestern Iran

Arezoo Zaker Moshfegh
Isfahan University of Technology
Hossein Khademi
hkhademi@cc.iut.ac.ir
Isfahan University of Technology https://orcid.org/0000-0003-2945-122X
Saeid Hojati
Shahid Chamran University of Ahvaz

Research Article

Keywords: Deposited atmospheric dust, Street dust, Date palm-associated dust, Dust contamination, Particle size distribution

Posted Date: November 4th, 2026

DOI: https://doi.org/10.21203/rs.3.rs-11414659/v1

License: This work is licensed under a Creative Commons Attribution 4.0 International License.
Read Full License

Comparative assessment of potentially toxic elements geochemistry in various dusts in Southwestern Iran

Abstract

Simultaneous measurements of the geochemical characteristics of different dust types remain limited. Direct sampling of atmospheric dust to assess potentially toxic element (PTE) concentrations is more costly and time-consuming compared to sampling other types of dust. The aim of this study was to investigate the relationships among acid-extractable PTE concentrations in deposited atmospheric dust (DAD), street dust (SD), and date palm-associated dust (DPAD), and to evaluate the potential of SD and DPAD to provide complementary information on PTE concentrations in DAD. Thirty-two DAD and 32 SD samples were collected seasonally from 12 cities in Khuzestan Province, southwestern Iran, over a one-year period, yielding a total of 128 samples for each dust type. Additionally, 32 DPAD samples were collected only once from the corresponding sites. Acid-extractable (pseudo-total) concentrations of Mn, Cd, Cu, Zn, Pb, Cr, Ni, and Co were measured using ICP-OES, particle size distributions were determined by laser diffraction, and data were analyzed using correlation, regression, principal component, and hierarchical cluster analyses. Mean PTE concentrations generally followed the order DAD > DPAD > SD, with DAD and DPAD exhibiting more similar values. DAD and DPAD contained higher proportions of fine silt, whereas SD contained a greater proportion of coarse silt. Correlation and regression analyses revealed element-dependent relationships among the three dust matrices. Mn showed weak and inconsistent correspondence, with low coefficient of determination ($R^2 \approx 0.01–0.10$). In contrast, Zn, Cr, and Co showed strong correspondence between DPAD and DAD, with R^2 values of 0.67-0.88. Relationships for Ni, Pb, Cu, and Cd varied according to the elements and dust-matrix pairs examined. SD also showed relatively strong correspondence with DPAD for selected elements, particularly Zn and Cu, although the strength of these relationships differed among elements. Overall, the results indicate that DPAD and SD may provide complementary information for assessing the geochemical characteristics of DAD, but the extent of this correspondence is element-dependent. Because DPAD was sampled only once, whereas DAD and SD were sampled seasonally, the observed relationships do not establish seasonal correspondence or direct transfer pathways among the matrices. Further multi-season and multi-site investigations, together with independent validation, are needed before the broader applicability of these relationships or the quantitative prediction of PTE concentrations in DAD can be established.

Keywords: Deposited atmospheric dust; Street dust; Date palm-associated dust; Dust contamination; Particle size distribution

1. Introduction

Dust is one of the most significant natural hazards in arid and semi-arid regions, influencing air quality, climate, ecosystem functioning, and human health through the transport and deposition of mineral particles and associated pollutants. The Middle East is the second-largest global source of mineral dust after North Africa, contributing approximately 15–20% of the world's dust emissions (Shao et al., 2011; Adebiyi et al., 2023). The primary sources of dust in the region include the Rub' al-Khali, al-Nafud, and al-Dhana deserts in Saudi Arabia, the Mesopotamian plains in Iraq, and extensive deserts, dry riverbeds, and desiccated wetlands across Iran (Jish Prakash et al., 2016; Karami et al., 2020, 2024; Hossein Hamzeh et al., 2021; Sabetghadam et al., 2021). Since these dust sources frequently affect densely populated and industrialized areas, understanding the occurrence and distribution of contaminants transported by dust has become an important environmental research priority.

Recent investigations have been focused on several environmental dust matrices, including atmospheric dust (e.g., Ebrahimi Khusfi et al., 2020; Proestakis et al., 2025; Soliman et al., 2025), street dust (e.g., Al-Khashman et al., 2024; Dehvari et al., 2025), indoor dust (e.g., Zhao et al. 2022; Buljovčić et al., 2024), and plant-associated dust (e.g., Naderizadeh et al. 2016; Bierza and Bierza, 2024). AD is made up of suspended particles that are lifted from the surface, particularly in arid and semi-arid regions, through wind-driven processes or tropospheric disturbances. These particles typically range from a few micrometers to several tens of micrometers in aerodynamic diameter and can remain airborne for prolonged periods. In contrast, street dust (SD), which contains natural and urban soil, construction materials, vehicle emissions, and industrial particulates, is a significant urban pollutant, especially in industrialized areas (Semerjian et al., 2021; Vlasov et al., 2022a). Street dust can transport contaminants over local to regional scales. Also, indoor dust refers to the accumulation of fine airborne particles (typically $\leq$ 100 μm) within indoor environments, originating from both outdoor sources (e.g., atmospheric particles, traffic emissions) and indoor sources such as building materials and human activities (Tan et al., 2016). In addition, plant-associated dust is defined as particulate matter that deposits on the surfaces of plant tissues such as leaves, stems, and fruits, where it may alter physiological and anatomical functions (Łukowski et al., 2020). Deposition of particulate matters on plant surfaces can ultimately influence plant health and ecosystem function (Farmer, 1993; Singh et al., 2022). Although each of these matrices provides valuable environmental information, they differ in their sources, accumulation mechanisms, and suitability for environmental monitoring.

DAD and SD are important carriers of potentially toxic elements such as Pb, Cd, Cr, Ni, Zn, and Cu commonly referred to as PTEs according to the critical analysis by Pourret and Hursthouse (2019). They can be resuspended by traffic and other disturbances, thereby affecting air quality, soil properties, and human health (Rehman et al., 2025; Öncü et al., 2025). Furthermore, deposition of particulate matter (PM)-bound PTEs on plant surfaces may contribute to the accumulation of toxic elements, potentially affecting physiological and biochemical processes (Singh et al., 2022).

Previous investigations have extensively characterized the concentrations, sources, and environmental risks of PTEs in individual dust matrices. Elevated concentrations of Cd, Pb, Cr, Ni, Zn, Cu, and other PTEs have frequently been reported in atmospheric and street dust from urban and industrial environments, with transportation-related emissions representing one of the principal anthropogenic sources (Isinkaralar et al., 2024a; Al-Khashman et al., 2024; Xia et al., 2025; Soliman et al., 2025; Rehman et al., 2025). Similarly, accumulation of PTEs on vegetation has been widely documented in industrial and traffic-affected areas (Bierza and Bierza, 2024). In southwestern Iran, previous studies have demonstrated considerable PTE contamination in soils, sediments, atmospheric particles, and street dust associated with fossil fuel combustion, oil and gas activities, regional dust storms, and urban emissions (Heidari-Farsani et al., 2013; Sadeghdoust et al., 2020; MalAmiri et al., 2022; Darvish Khatooni et al., 2026). Naderizadeh et al. (2016) further showed that dust accumulated on date palm leaves reflects spatial variations in atmospheric PTE contamination, highlighting its potential value as an environmental monitoring medium.

Despite these advances, most previous studies have examined atmospheric dust, street dust, or plant-associated dust independently. Consequently, limited information is available regarding the relationships among PTE concentrations in these different dust matrices or the extent to which readily accessible materials such as street dust and date palm-associated dust (DPAD) can reflect PTE concentrations in atmospheric dust. Addressing this question is important because direct collection of atmospheric dust requires specialized equipment, carefully selected sampling locations, extended collection periods, and favorable environmental conditions, all of which limit sampling frequency and spatial coverage. In contrast, street dust and plant-associated dust can be collected rapidly, economically, and throughout the year, making them attractive candidates for complementary or surrogate environmental monitoring if robust relationships with atmospheric dust can be established.

Accordingly, this study presents, to the best of our knowledge, the first comprehensive comparative assessment of PTEs in deposited atmospheric dust, street dust, and date palm-associated dust collected from southwestern Iran. The objectives were (i) to compare the geochemical characteristics of PTEs among the three dust matrices, (ii) to evaluate the relationships between PTE concentrations in atmospheric dust and those measured in street dust and DPAD, and (iii) to assess the potential of these readily available dust matrices as complementary indicators for atmospheric dust monitoring. By integrating comparative geochemical analysis with evaluation of inter-matrix relationships, this study provides new insights into both the environmental behavior of PTEs and practical approaches for dust monitoring in arid environments.

2. Materials and Methods

2.1 Study area

The study area is located in Khuzestan Province, southwestern Iran, bordering Iraq to the west and the Persian Gulf to the south (Figure 1). Covering approximately 63,238 km² and supporting a population of about 4.7 million (Statistical Center of Iran, 2025)**,** Khuzestan is one of Iran's largest and most industrialized provinces. Elevation ranges from sea level to about 3,700 m above sea level, resulting in climatic variations from arid and semi-arid conditions in the southern regions to semi-humid conditions in the north. The prevailing winds are predominantly northwesterly to westerly in the southern and western parts of the province (Abadan, Khorramshahr, and Shadegan) whereas more variable wind directions occur in the northern cities including Dezful, Shush, and Shushtar. The province contains seven major internal dust sources (Parno et al., 2024), mainly formed due to wetland desiccation, reduced river discharge, and land-use change (Yousefi-Kebriya et al., 2025). In addition, transboundary dust originating from Iraq, Saudi Arabia, and Kuwait significantly contributes to atmospheric dust loading across the region (Salmabadi et al., 2023).

Sampling was conducted in urban and rural areas of Ahvaz, Abadan, Khorramshahr, Shadegan, Karoon, Hamidiyeh, Bavi, Shushtar, Gotvand, Shush, Karkheh, and Dezful (Figure 1). These locations represent a wide range of environmental conditions with respect to dust intensity, land use, industrial activity, population density, and pollution characteristics**.** Major industries such as the National Iranian South Oil Company, Khuzestan Steel Company, refineries, petrochemical complexes, alcohol production plants**,** food-processing industries, thermal and hydroelectric power plants, as well as extensive sugarcane agro-industrial farms

and irrigated and rainfed agriculture**,** are concentrated in these areas, representing important potential sources of atmospheric pollution. Ahvaz, the provincial capital, has repeatedly been reported among the world's most particulate-polluted cities based on PM_{10} concentrations (Hamidi et al., 2025). The study area was therefore selected because it combines frequent dust events multiple natural and anthropogenic sources of particulate matter, and extensive date palm plantations that provide suitable surfaces for long-term dust accumulation. These characteristics make Khuzestan an appropriate natural laboratory for evaluating relationships among atmospheric dust, street dust, and date palm-associated dust, as well as their potential application in environmental monitoring.

2.2 Sampling

2.2.1 Deposited atmospheric dust (DAD) sampling

Deposited atmospheric dust (DAD) samples were collected seasonally over one year from 32 sampling sites distributed across the studied counties (Table 1). The selected sites represented industrial zones, urban locations with heavy traffic, and rural settlements. Counties with larger populations and greater spatial extent were assigned proportionally more sampling sites than less populated counties to improve the spatial representation of the study area. During the one-year sampling period, the study area experienced pronounced seasonal climatic variation, with hot, predominantly dry conditions during the warmer months and cooler, relatively more humid conditions during the colder months, when most rainfall occurred. Wind conditions varied across the study area, and dust events occurred intermittently throughout the year, with their frequency varying by location and month, according to meteorological data obtained from the Islamic Republic of Iran Meteorological Organization (IRIMO, 2026).

The DAD collectors consisted of modified ceramic traps developed from the conventional glass traps described by Hojati et al. (2012). These traps were designed to improve stability against wind, heat, and breakage, and to facilitate easier handling in the field. The development and application of these traps were based on the researcher’s field experience under the harsh climatic conditions of Khuzestan, showing greater durability and reduced sampling error compared with glass and tile traps. Each trap consisted of four ceramic plates, each measuring 0.6 × 0.6 m, providing an effective collection surface area of 1.44 m^2. The plates were covered with a 2 × 2 mm plastic mesh to retain deposited particles, while a nylon layer beneath the mesh minimized the loss of deposited materials (Figure 2).

The traps were installed on the rooftops of one- or two-story buildings at heights of approximately 3–6 m above ground level. This installation height was selected to reduce contamination from local ground resuspension, pedestrian activity, and splash while allowing

efficient collection of deposited atmospheric dust under natural environmental conditions (Norouzi and Khademi, 2015). Before the beginning of each seasonal sampling period, all ceramic plates, meshes, and collection components were thoroughly cleaned with distilled water, air-dried, and reassembled to minimize cross-contamination between consecutive sampling periods. After each seasonal collection, the deposited material was completely removed before the traps were reinstalled.

Deposited dust particles were collected at the end of each dry season (spring and summer) using a clean soft brush and at the end of each wet season (autumn and winter) using a clean rubber wiper to facilitate recovery of fine particles adhering to the trap surface. A total of 128 DAD samples (32 sites representing important potential sources of 4 seasons) were collected during the study (Table 1).

2.2.2 Street dust (SD) sampling

Street dust (SD) samples were collected seasonally from locations adjacent to each DAD sampling site traps including sidewalks, parking areas, and flat road surfaces that represented the local depositional environment. At each site, approximately 150 g of loose surface dust was collected from a 2 × 2 m plot using a clean plastic brush. Sampling was conducted only on dry surfaces, while areas affected by recent rainfall, sweeping, visible litter, or coarse debris were avoided to minimize potential contamination and ensure sample consistency.

To prevent cross-contamination among sampling sites, plastic brushes and other sampling equipment were thoroughly washed with distilled water, air-dried, and cleaned before reuse. The collected samples were immediately transferred to clean polyethylene containers and transported to the laboratory. Thirty-two SD samples were collected during each season, resulting in a total of 128 samples over the one-year sampling period (Table 1).

2.2.3 Date palm associated dust (DPAD) sampling

Dust deposited on the leaves of Berhi and Estamaran date palm cultivars was sampled once at the end of winter from the nearest palm trees to each DAD and SD sampling site. The number of DPAD samples collected in each county was identical to that of the corresponding DAD and SD sampling sites, resulting in a total of 32 samples. At the time of DPAD sampling at the end of winter, the study area experienced relatively mild conditions, with limited precipitation and intermittent dust events across the sampling locations, according to meteorological data obtained from the Islamic Republic of Iran Meteorological Organization (IRIMO, 2026).

Dust was gently removed from the upper surfaces of 3–5 mature leaves per tree at a height of approximately 1.5–2 m above ground using a clean plastic spatula while wearing disposable gloves to minimize contamination.

Unlike deposited atmospheric dust and street dust, which were collected seasonally to characterize temporal variability, DPAD was sampled only once because dust retained on perennial date palm leaves represents cumulative atmospheric deposition over several months. Moreover, seasonal collection of DPAD would not yield sufficient sample for laboratory analyses. Consequently, DPAD provides an integrated record of dust deposition rather than seasonal deposition. This difference in sampling frequency should be considered when interpreting correlations and regression analyses among the three dust matrices and is further discussed as a limitation of the study.

Table 1 summarizes the number of DAD, SD, and DPAD samples collected from each county.

2.2.4 Background soil sampling

Background soil samples were collected during the study from seven locations situated in remote rural areas with limited anthropogenic influence and located away from major roads, industrial facilities, and urban settlements. These sites were chosen to provide representative local geochemical background conditions for comparison with the collected dust samples.

Soil samples were taken from a depth of 5–25 cm, once during the year, in undisturbed areas to minimize the influence of recent surface contamination. Approximately 2 kg of composite soil was obtained from each site and used as the regional geochemical baseline. These soils served as geochemical baselines for comparison with DAD, SD, and DPAD, providing a regional geochemical background for comparison with the dust samples and helping to contextualize their elemental concentrations.

2.3 Sample preparation

After sampling, all dust and soil samples were air-dried, sieved through a 2 mm sieve to remove coarse debris, pebbles, and organic residues, and finally stored in sealed plastic containers at room temperature before being transferred to the laboratory for analysis.

2.4 Laboratory Analysis

2.4.1 Acid digestion and chemical analysis

Acid-extractable concentrations of potentially toxic elements (PTEs) were determined following the USEPA Method 3050B acid digestion procedure (U.S. Environmental Protection Agency, 1996). This method provides pseudo-total (acid-extractable) rather than total elemental concentrations because it does not completely dissolve silicate minerals. The procedure was selected because the objective of this study was to evaluate environmentally available PTEs using a standardized and widely accepted environmental protocol rather than to determine the total elemental inventory of the mineral matrix.

Approximately 0.5 g of each homogenized dust or soil sample was transferred into a Teflon digestion vessel containing 10 ml of 6N nitric acid and allowed to pre-digest at room temperature for 48 hours. The samples were then heated at 95°C for 30 minutes to complete the digestion process. After cooling, the digests were filtered through Whatman No. 42 filter paper to remove undissolved mineral residues and other insoluble particles remaining after acid digestion. The filtrates were transferred to a 50-ml volumetric flask and diluted to volume with deionized water prior to elemental determination.

Before use, all glassware, digestion vessels, and plastic containers were soaked in dilute nitric acid and thoroughly rinsed with double-distilled water to minimize contamination. All reagents were of analytical grade (Merck, Germany). Standard calibration solutions for each element were prepared by serial dilution of 1000 mg l^{-1} stock solutions and calibration curves were established within the working concentration ranges. Acid-extractable concentrations of Mn, Cu, Zn, Pb, Co, Cr, Cd, and Ni were determined using an inductively coupled plasma optical emission spectrometer (ICP-OES;Spectro Genesis). All measurements were performed in triplicate together with procedural blanks.

2.4.2 Particle-size analysis

Representative samples of the three different dust types were selected for particle-size analysis using a Malvern Hydro 2000 g laser diffraction particle-size analyzer capable of high-resolution analysis of small samples. Prior to particle-size distribution analysis, samples were dispersed in 1 M sodium hydroxide and 10% sodium hexametaphosphate solution following the procedures described by McTainsh et al. (1997) and Hojati et al. (2012). These dispersing agents were used to minimize particle aggregation and ensure complete dispersion of individual particles before analysis.

Particle-size distributions were determined by laser diffraction and quantified using the instrument software as the relative percentages of particles within predefined equivalent particle-diameter classes. These included the conventional soil textural fractions (sand, silt,

clay, and different fractions of silt and sand) together with the cumulative proportions of particles having equivalent diameters <2.5 μm, <5 μm, and <10 μm. The latter terminology is used throughout this manuscript to distinguish laser-diffraction size classes from aerodynamic particulate matter fractions ($PM_{2.5}$, PM_5, and PM_{10}) obtained using size-selective air samplers.

Because particle-size analysis was conducted on representative subsets of the collected samples the number of samples analyzed for particle-size distribution was smaller than the total number of collected dust samples and differed among the three dust types. Particle-size analysis was performed on 18 DAD, 11 SD, and 30 DPAD samples. The corresponding sample sizes used in subsequent statistical analyses are reported in the relevant tables.

2.4.3 Quality assurance and quality control

Quality assurance and quality control (QA/QC) procedures were implemented throughout the analytical process. A certified reference material (San Joaquin soil, Standard # 2709) from the National Institute of Standards and Technology (NIST), USA, was analyzed together with the study samples to evaluate analytical accuracy. Recovery rates of different metals ranged from 87% to 103%, while relative standard deviations were below 5%, indicating satisfactory analytical precision and repeatability. Procedural blanks were included throughout the analytical sequence to monitor potential contamination.

2.5 Data Analysis

Prior to statistical analyses, all datasets were screened for outliers using the boxplot/interquartile range (IQR) method. Outlier detection was performed before correlation, regression, and comparative statistical analyses. Only observations identified as statistical outliers according to the IQR criterion were excluded from analyses requiring complete paired datasets. Consequently, the number of observations used in individual statistical analyses may differ from the total number of collected samples, and the corresponding sample sizes are reported in the relevant tables and figures.

For deposited atmospheric dust (DAD) and street dust (SD), the concentration of each potentially toxic element (PTE) at each sampling site was calculated as the mean of four seasonal measurements, each determined in triplicate. These annual mean values were subsequently paired with the corresponding date palm-associated dust (DPAD) measurements collected from the same locations, resulting in 32 paired observations for each dust type.

Descriptive statistics, including minimum, maximum, mean, and standard deviation, were calculated for all PTEs in each dust matrix.

Prior to applying parametric statistical methods, data normality was evaluated using both the Kolmogorov–Smirnov and Shapiro–Wilk tests. Homogeneity of variances was assessed before performing analysis of variance (ANOVA). When these assumptions were satisfied, differences among dust types were evaluated using one-way ANOVA followed by the Least Significant Difference (LSD) test for pairwise comparisons. For variables that did not satisfy normality assumptions, non-parametric analyses were considered during correlation analysis through Spearman's rank correlation coefficient. Statistical significance was assessed at $p < 0.05$, while $p < 0.01$ was considered to indicate stronger statistical evidence. Relationships among PTE concentrations in DAD, SD, and DPAD were investigated using pairwise simple linear regression analyses between DAD–SD, DAD–DPAD, and SD–DPAD. For each regression model, the unstandardized slope coefficient (B_1), its standard error (SE), intercept (B_0), coefficient of determination (R^2), significance level (p-value), and sample size (N) were determined. Regression residuals were also examined as part of model diagnostics, and the range of standardized residuals was reported for each model. The corresponding regression equations were presented in the regression figures. In addition, Pearson's correlation coefficient was used for normally distributed variables, whereas Spearman's rank correlation coefficient was applied to variables that deviated from normality. Correlation and regression analyses were performed after outlier screening.

In addition, particle size distributions of the three dust types (DAD, SD, and DPAD) were summarized using descriptive statistics, including minimum, maximum, mean, and standard deviation for various particle size categories ranging from clay (<0.002 mm) to very coarse sand (1-2 mm), together with cumulative proportions of particles having equivalent diameters <2.5 μm, <5 μm, and <10 μm, as determined by laser diffraction. Relationships between PTE concentrations and particle-size characteristics were evaluated using Pearson or Spearman correlation analyses, depending on data distribution. Regression analyses were also performed to examine the influence of particle-size fractions on PTE concentrations, and the corresponding R^2 values were calculated to evaluate the proportion of explained variance.

Principal component analysis (PCA) was performed to investigate the multivariate structure and covariation patterns among the eight PTEs (Mn, Cd, Co, Cr, Cu, Ni, Pb, and Zn) across the three dust types. Data from deposited atmospheric dust (DAD), street dust (SD), and date palm-associated dust (DPAD) were analyzed as a pooled dataset. The suitability of the dataset for PCAwas assessed using the Kaiser–Meyer–Olkin (KMO) measure of sampling

adequacy and Bartlett's test of sphericity. Components were retained according to the eigenvalue > 1 criterion, with the scree plot also examined to support component retention. To improve interpretability, the retained components were subjected to Varimax rotation with Kaiser normalization. Rotated component loadings, communalities, and the proportion of explained variance were used to characterize the component structure. Component scores were subsequently calculated for individual observations, and a PCA score plot was constructed to examine the distribution patterns of the three dust types. Because DAD, SD, and DPAD observations were spatially matched by sampling location, differences in component scores among the three dust types were evaluated using the Friedman test at a significance level of $p < 0.05$. When the Friedman test indicated a significant difference, pairwise comparisons were performed using the Wilcoxon signed-rank test with Bonferroni correction.

To further examine similarities and grouping patterns among the PTEs and to assess the consistency of the resulting structure with PCA, hierarchical cluster analysis (HCA) was also performed. Before performing cluster analysis (CA), the heavy metal concentration data were standardized by means of z-scores to calculate Euclidean distances for similarities in the variables. Finally, hierarchical cluster analysis was carried out using Ward's method on the standardized data set (Lu et al., 2010). Similarities and hierarchical associations among the PTEs were evaluated from the resulting cluster structure and visualized using a dendrogram.

All statistical analyses were performed using IBM SPSS Statistics (IBM Corp., Armonk, NY), version 27 (IBM Corp, 2024).

3. Results

3.1 Descriptive statistics

The descriptive statistics (Table 2) showed differences in concentration ranges, coefficients of variation, and distributional characteristics among DAD, SD, and DPAD. Mn, Co, Ni, and Cr generally showed lower coefficients of variation and distributions closer to normality across the three dust types. This might be due to their constant presence in the atmosphere, from local and distant sources. In contrast, Cu, Pb, Zn, and Cd showed greater variability and more asymmetric distributions. Asymmetric distribution may reflect heterogeneous sources and processes affecting the distribution of element among the dust matrices. Overall, the comparison of means, ranges, and variability indicators demonstrates that while some elements have similar mean concentrations across DAD, SD, and DPAD, their distributional structures and fluctuation patterns are not consistent. Therefore, the upcoming

correlation analysis (Pearson or Spearman) is expected to uncover varying degrees of association among the dust types and individual elements.

3.2 Correlation structure and regression models

Table 3 presents the correlation coefficients and significance calculated for the three pairwise comparisons among dust types (DAD – SD, DAD – DPAD, and SD – DPAD). The regression results are interpreted primarily as measures of association and shared variability within the present dataset rather than as evidence of direct transport pathways or causal relationships.

Despite the simultaneous seasonal collection of DAD and SD, and the annual cumulative sampling of DPAD, the correlation patterns (Table 3) and the linear regression models (Figure 4a, Table 4) indicate that Mn exhibits no coherent, stable, or reliable relationships among the three dust types. The weak, negative, and statistically insignificant correlation coefficients, together with the very low coefficients of determination across dust matrices ($R^2 \approx 0.01–0.10$), demonstrate that neither SD nor DPAD can provide a sufficiently consistent basis for estimating Mn concentrations in DAD within the present dataset. As shown in Figure 3a, the mean concentration of Mn was highest in DAD, although the difference between DAD and DPAD was not statistically significant. Overall, the correlation and regression results indicated weak and statistically non-significant correspondence among the three dust matrices for Mn.

In contrast, Cd displays a more consistent behavior. The mean concentrations of Cd in DAD, SD, and DPAD fall within a narrow range, with no statistically significant differences among them (Figure 3b). These concentrations are lower than the Netherlands soil guideline (R2) but higher than the USEPA threshold (R1) and the local background (R3), indicating deposition beyond natural levels. Despite this homogeneity, the regression patterns among dust matrices (Figure 4b) reveal important distinctions. The positive and significant DAD–SD relationship, accompanied by $R^2 \approx 0.28$, suggests that part of the variability in SD is influenced by atmospheric inputs. In contrast, DAD–DPAD shows the weakest relationship ($R^2 \approx 0.10$), implying that short-term fluctuations in DAD are not directly reflected in Cd accumulation on leaves, where processes such as surface retention, wash-off, and resuspension exert stronger control. The relatively strong correlation between Cd concentrations in SD and DPAD ($\rho \approx 0.76$; $R^2 \approx 0.68$) suggests a degree of geochemical correspondence between these matrices. However, this association alone does not establish a direct transfer pathway or demonstrate that street

dust is a dominant source of Cd on date palm leaves. Previous studies in industrial cities have reported elevated Cd levels in SD and DAD and classified Cd as a high-risk urban metal (Cai and Li, 2019).

Co and Cr showed comparatively strong relationships between DAD and DPAD. The concentrations of Co exceeded the reference values considered in this study (R1, R2, and R3), while Cr concentrations exceeded R1 and R3. In both cases, the concentration sequence was generally DAD > DPAD > SD. A strong positive association was observed between DAD and DPAD for Co ($r = 0.831$, $p < 0.001$; $R^2 = 0.691$) and Cr ($\rho = 0.888$, $p < 0.001$; $R^2 = 0.885$) (Table 3; Figure 4c and 4d; Table 4). These relationships indicate a high degree of correspondence between DAD and DPAD for these two elements. However, the association should not be interpreted as proof of direct atmospheric transfer because both natural mineral material and anthropogenic inputs may contribute to their concentrations.

Rana et al. (2024) reported high concentrations of Cr and Co in SD and DAD from industrial regions of Bangladesh, identifying traffic and industrial activities as the main sources of Cr in SD. These elements were also commonly found in deposited atmospheric particulates. Similarly, observations from Huizhou, China, show that PTEs such as Cr and sometimes Co, in dust accumulated on leaf surfaces reflect atmospheric inputs and direct deposition onto vegetation. Dust deposited on leaves effectively integrates airborne particulate composition, especially for metals of atmospheric and urban origin (Qiu et al., 2009).

Cu exhibited a more complex pattern compared to Co and Cr. Although Cu concentrations in all three types of dust significantly exceeded the R1, R2, and R3 thresholds (Figure 3e), indicating elevated levels across the region, its transfer dynamics were less straightforward. While the DAD–SD and DAD–DPAD correlations were statistically significant, they had low explanatory power. In contrast, the SD–DPAD relationship was very strong and highly significant ($R^2>0.57$), indicating that SD explains more than half of the variation in DPAD Cu concentrations (Table 3; Figure 4e; Table 4). The relatively strong correspondence between Cu concentrations in street dust and date palm-associated dust suggests that these matrices may share some geochemical characteristics or sources. However, the observed relationships do not establish direct transfer pathways, and the comparatively weaker correspondence between Cu in DAD and DPAD does not, by itself, demonstrate that atmospheric deposition plays a lesser role than for Co and Cr.

Ni showed the highest concentration in DAD and the lowest concentration in SD (Figure 3f). The concentrations exceeded R1 and R3. A significant positive association was observed between DAD and SD ($R^2 \approx 0.29$), while the DAD–DPAD relationship was weaker ($R^2 \approx 0.18$). No statistically significant association was detected between SD and DPAD. These results indicate only moderate and inconsistent correspondence among the matrices for Ni and do not support the use of SD or DPAD as a reliable quantitative indicator of DAD Ni concentrations.

. According to Su et al. (2026), the primary source of PTEs in rooftop dust is largely influenced by an unidentified source (67.4%), whereas ground-level dust is mainly affected by combustion sources (42.4%) and traffic emissions (18.2%). This vertical heterogeneity indicates that rooftop dust reflects regional-scale atmospheric deposition, while ground dust represents local pollution signals. According to the findings of Ahmed et al. (2026), three dominant sources contributing to the loading of PTEs, including Ni, in road dust from metro bus stations in Lahore were identified as mixed traffic–industrial emissions, non-exhaust vehicular emissions, and mixed urban deposition.

Pb concentrations in all three dust matrices were high and exceeded R1, R2, and R3 thresholds (Figure 3g). The DAD–DPAD relationship was significant and had the highest R^2 ($\approx$0.28). This suggests that leaves serve as accumulative surfaces where short-term DAD fluctuations are not directly reflected. The DAD–SD relationship was also significant but explained a relatively small proportion of the variance ($R^2 = 0.129$), whereas the SD–DPAD relationship was not statistically significant ($R^2 \approx 0.08$). Thus, although DPAD showed greater correspondence with DAD than SD for Pb, the relatively low R^2 values indicate limited explanatory capability.

Naderizadeh et al. (2016) documented measurable concentrations of Ni and Pb on palm leaves, with Pb being strongly influenced by anthropogenic sources, while Ni in DAD was mainly linked to natural origins. Isinkaralar et al. (2024b) reported significant spatial variability of Ni and Pb in SD in Ankara, attributing it to anthropogenic inputs. Their findings highlight that correlations with DAD may vary from moderate to weak depending on deposition processes and local conditions.

Zn showed a relatively consistent pattern of correspondence among the three dust matrices. Zn concentrations in all three media exceeded R1, R2, and R3 by a considerable margin (Figure 3h), and the concentrations followed the sequence of DAD > DPAD > SD. Unlike other

462 elements, all pairwise correlations (DAD–SD, DAD–DPAD, SD–DPAD) were very strong and
463 statistically significant (Table 3, Figure 4h, Table 4). The coefficients of determination were
464 approximately 0.46 for DAD–SD, 0.67 for DAD–DPAD, and 0.35 for SD–DPAD. Among the
465 investigated elements, Zn therefore showed one of the most consistent patterns of
466 correspondence among the three matrices. Nevertheless, these relationships describe the
467 present dataset and should not be interpreted as demonstrating a causal transfer pathway or as
468 providing externally validated prediction.

469 According to Li et al. (2021), Zn is identified as one of the predominant anthropogenic
470 metals in urban areas and is closely linked to fine airborne particulates that efficiently settle
471 and build up on leaf surfaces. Studies conducted at the Yazd bus terminal in Iran (Esfandiari
472 and Hakimzadeh, 2022) similarly showed substantial Zn enrichment on leaf-deposited dust,
473 primarily attributed to traffic emissions and atmospheric particulates. The high accumulation
474 of Zn in leaf-surface dust was attributed to the effective deposition of fine atmospheric
475 particles, suggesting that DPAD may have potential complementary monitoring value for
476 atmospheric Zn pollution.

477 **3.3 Multivariate analysis**

478 Principal component analysis (PCA) was performed to evaluate the multivariate structure
479 of the dataset and to complement the pairwise correlation analyses. The Kaiser–Meyer–Olkin
480 (KMO) measure was 0.811, while Bartlett's test of sphericity was significant ($\chi^2 = 467.564$, df
481 $= 28$, $p < 0.001$), indicating that the dataset was suitable for PCA.

482 Two principal components with eigenvalues >1 were retained and together explained
483 71.64% of the total variance (Table 5). Following Varimax rotation, PC1 accounted for 47.95%
484 of the variance and was characterized mainly by Cd (loading = 0.899), Cu (0.871), Pb (0.824),
485 Co (0.771), Cr (0.717), and Zn (0.637). PC2 explained 23.69% of the variance and was
486 dominated by Mn (0.875) and Ni (0.841), while Co and Cr also showed moderate contributions
487 (Table 6).

488 The PCA score distribution showed substantial overlap between DAD and DPAD, whereas
489 SD was comparatively more separated. Statistical comparison of the PCA scores indicated
490 significant overall differences among the matrices for both PC1 ($\chi^2 = 13.000$, $p = 0.002$) and
491 PC2 ($\chi^2 = 35.688$, $p < 0.001$). In the Bonferroni-adjusted pairwise comparisons, DAD and
492 DPAD did not differ significantly for PC1 ($p = 0.411$). Their PC2 comparison also did not

493 remain significant after Bonferroni adjustment ($p = 0.020$; adjusted $\alpha = 0.0167$). In contrast,
494 SD differed significantly from both DAD and DPAD for PC1 ($p = 0.006$ and $p = 0.002$,
495 respectively) and for PC2 (both $p < 0.001$) (Table 7).

496 The cluster analysis (CA) results for the PTEs are shown in Figure 7 as a dendrogram.
497 Hierarchical cluster analysis (HCA) separated the eight PTEs into two major clusters. The first
498 cluster comprised Cd, Cu, Co, Cr, Pb, and Zn, with particularly close associations between Cd–
499 Cu and Cr–Pb, whereas the second cluster consisted exclusively of Mn and Ni. The two major
500 clusters merged only at a relatively high rescaled distance, indicating a distinct multivariate
501 behavior of Mn and Ni compared with the other PTEs. This clustering pattern was highly
502 consistent with the PCA results, in which Cd, Cu, Pb, Co, Cr, and Zn were primarily associated
503 with PC1, while Mn and Ni showed the highest loadings on PC2. The distance axis explains
504 the level of association between groups of variables. In the dendrogram, smaller linkage
505 distances indicate greater similarity between variables, whereas larger distances indicate less
506 similarity (Taghipour et al., 2011).

507 The PCA and HCA results provide complementary evidence for the multielement structure
508 of the dataset. However, these multivariate analyses do not, by themselves, provide sufficient
509 evidence to assign the elements to specific natural or anthropogenic sources. The observed
510 grouping may reflect a combination of common sources, particle-size characteristics,
511 atmospheric transport, geochemical associations, and post-depositional processes.

512

513 **3.4 Particle size characteristics and relationship with PTE concentrations**

514 The particle size distribution for all types of dust is presented in Table 8 and Figure 8, and
515 their correlations with PTEs are given in Table 9.

516 Descriptive statistics of particle-size distribution for the different types of dust (Table 8
517 and Figure 8) show that in all three types of dust, the percentage of silt is higher than that of
518 other particle-size classes. The total silt content was approximately 81.5% in DAD, 82.5% in
519 DPAD, and 54.1% in SD, whereas the corresponding sand fractions were approximately 4.3%,
520 2.7%, and 39.0%, respectively. Thus, DAD and DPAD generally contained finer material than
521 SD.

Table 8 and Figure 8 demonstrate that the particle-size distribution can influence the concentration of PTEs in various types of dust. DAD and DPAD, which have finer particles with higher proportions of clay and silt, naturally contain higher concentrations of PTEs compared to SD, which consists of coarser particles with a higher sand content. Additionally, as shown in Figure 3, the sequence of element concentrations follows the order of DAD, DPAD, and SD. This aligns with the basic principle of increased specific surface area and adsorption capacity in finer particles.

Mn is commonly associated with lithological and natural sources, and its distribution may also be related to particle-size characteristics. As shown in Table 9, Mn concentration was significantly and positively correlated with silt ($r = 0.446$) and the combined clay + fine-silt fraction ($r = 0.368$), whereas significant negative correlations were observed with sand ($r = -0.434$) and the combined coarse-silt + sand fraction ($r = -0.368$). In contrast, the correlation between Mn and clay alone was weak and not statistically significant ($r = 0.145$).

Despite the variability in the relationships presented in Table 9, particle size appears to be associated with the concentrations of several PTEs, although the strength of this association differed considerably among individual PTEs. Ni showed the clearest particle-size dependence, with significant positive relationships with finer fractions and negative relationships with coarser fractions. Similar directional patterns were observed for Co and, to a lesser extent, Cu and Mn. Although the corresponding R^2 values were generally low to moderate, the significant relationships and their consistent directions suggest that particle-size characteristics may partly contribute to the distribution of these PTEs in dust. In contrast, Cd, Cr, and Zn showed predominantly weak and non-significant relationships with particle-size fractions, while Pb exhibited only limited evidence of particle-size dependence. These differences indicate that factors other than particle size, including source characteristics, chemical speciation, mineralogical associations, and post-depositional processes, may also influence PTE concentrations. Overall, particle size appears to be an important contributing factor for some PTEs, particularly Ni and Co, but it cannot be considered a universal controlling factor for PTE concentrations in the investigated dust matrices.

These results indicate that particle-size composition is associated with the concentrations of several PTEs in the investigated dust matrices. However, the relatively low R^2 values for many of the relationships indicate that particle size alone does not explain most of the

554 variability in PTE concentrations. Therefore, particle size should be considered one of several
555 potentially relevant factors rather than the single controlling factor.

556 Therefore, in the cities under study, which, in addition to high population and traffic,
557 contain numerous factories and oil, gas, and steel industries, the elevated concentrations of
558 elements in various types of dust are significantly linked to industrial pollution sources (factory
559 emissions, steel industries, petrochemical complexes, and refineries), traffic (vehicle exhaust,
560 tire wear, and brake abrasion), and other human activities. These sources introduce elements
561 into the dust cycle whose nature and behavior go beyond particle size alone. Factors such as
562 the presence of organic matter, soot compounds, and the chemical characteristics of forming
563 phases (such as PTEs in exhaust soot or abrasion particles) influence the adsorption and
564 transport of these elements. Therefore, while particle size is an important physical factor, the
565 complex combination of diverse emission sources and the chemical–physical characteristics of
566 particles ultimately determines the dispersion pattern and final outcome.
567

568 ## 3.4 Comparison with previous investigations

569 Comparison with previously reported concentrations showed that several PTEs, particularly
570 Mn, Co, Cu, Pb, and Zn, occurred at relatively high concentrations in the dust samples of the
571 present study (Table 10). Mn concentrations in all three dust types (1250.50–1651.59 mg kg^{-1})
572 were substantially higher than those reported for dust and surface soils in the comparative
573 studies, including those from Ahvaz, Bushehr, Khuzestan, and Ramhormoz. Co concentrations
574 in DAD, DPAD, and SD (38.82, 38.08, and 31.59 mg kg^{-1}, respectively) were also higher than
575 the values reported for dust from Bushehr and Dezful. Similarly, Pb concentrations in the
576 present samples (110.27–139.81 mg kg^{-1}) exceeded those reported for street dust from Ahvaz,
577 Dezful, Abadan, and Khorramshahr.

578 However, the comparative pattern varied among PTEs. Cr concentrations in the present
579 study (54.62–64.44 mg kg^{-1}) were comparable to some regional surface-soil values but
580 considerably lower than those reported for DAD in Dezful (393.53 mg kg^{-1}) and Abadan (134.2
581 mg kg^{-1}). Zn concentrations (231.85–305.69 mg kg^{-1}) generally fall within the range reported
582 for regional street dust and were close to that reported for Ahvaz (308.9 mg kg^{-1}). Cd
583 concentrations (0.56–0.61 mg kg^{-1}) were also broadly comparable with several regional values
584 and substantially lower than that reported for DAD in Dezful (1.25 mg kg^{-1}). Overall, the
585 comparison indicates an element-specific pattern, with the relatively elevated concentrations

of Mn, Co, and Pb being among the most notable characteristics of the dust samples analyzed in the present study.

4. Discussion

4.1 Overall differences among DAD, SD, and DPAD

The primary objective of this study was to evaluate whether SD and DPAD could provide useful complementary indicators of the elemental composition of DAD. The combined correlation, regression, particle-size, and multivariate results demonstrate that the degree of correspondence is strongly element-dependent.

The investigated elements can broadly be considered in three groups according to their correspondence among the three matrices. Mn showed weak and generally non-significant relationships, indicating that neither SD nor DPAD provides a consistent indicator of DAD Mn concentrations. Ni, Pb, and Cd showed limited to moderate and variable correspondence, with relatively low coefficients of determination in several comparisons. In contrast, Cr, Co, and Zn showed stronger correspondence between DAD and DPAD, while Cu displayed an intermediate pattern.

These differences indicate that the suitability of SD and DPAD as complementary indicators cannot be generalized to all PTEs. Instead, their usefulness depends on the individual element and on the processes governing its occurrence, transport, deposition, retention, and redistribution among the three matrices.

4.2 Statistical relationships and surrogate potential

The correlation and regression analyses provide quantitative measures of correspondence among the matrices, but they should not be interpreted as evidence of causality. A statistically significant relationship indicates that two variables vary together within the sampled dataset; it does not establish that one matrix causes the variation in another or identify a unique transport pathway.

This distinction is particularly important because several significant relationships in the present study had relatively low R^2 values. Such relationships may be statistically detectable while still having limited explanatory or predictive value. Therefore, the regression results should be regarded as evidence of the degree of correspondence observed in the present dataset rather than as independently validated predictive models.

Mn represents the clearest example of weak correspondence. Its relatively low and non-significant relationships among the matrices suggest that factors other than simple correspondence between deposited dust, street dust, and leaf-deposited dust contribute substantially to its observed variability. The relatively consistent occurrence of Mn in environmental dust may reflect contributions from mineral material and other sources, but the present association analyses cannot distinguish among these possibilities.

Ni, Pb, and Cd showed more variable relationships. The moderate DAD–SD relationship observed for Ni, together with the weaker DAD–DPAD relationship and absence of a significant SD–DPAD relationship, indicates that correspondence among matrices is not sufficiently consistent to support reliable quantitative estimation. For Pb, the stronger DAD–DPAD relationship relative to the other pairwise comparisons suggests that DPAD may contain useful information concerning deposited Pb; however, the relatively low R^2 indicates that substantial unexplained variability remains.

Cd is particularly interesting because the SD–DPAD relationship was relatively strong despite the weaker DAD relationships. This may indicate that common surface-related processes or similar source contributions influence Cd in SD and DPAD. However, this pattern alone cannot establish a specific source or mechanism. The lack of a strong particle-size relationship for Cd further suggests that factors other than grain-size distribution may contribute to its distribution among the matrices.

The strongest correspondence was observed for Cr, Co, and Zn, particularly between DAD and DPAD. The high DAD–DPAD coefficients for Cr and Co indicate that variation in their concentrations was closely aligned between the two matrices. This finding is consistent with the possibility that DPAD can retain information related to atmospheric deposition for these elements. Nevertheless, the correspondence does not demonstrate direct transfer from DAD to leaves because both matrices may be affected by common environmental inputs and by processes occurring before or after deposition.

Zn showed particularly consistent relationships among all three matrices, with the strongest DAD–DPAD correspondence among the Zn comparisons. This result supports the potential use of DPAD as a complementary indicator of atmospheric Zn deposition in the study area. However, independent validation using direct atmospheric-deposition measurements would be required before applying this relationship for quantitative prediction beyond the present dataset.

Cu showed an intermediate pattern. Its significant relationships with DAD and relatively strong SD–DPAD association indicate appreciable correspondence among the matrices, but the relatively modest explanatory power of some DAD relationships suggests that Cu behavior is more complex than a simple one-to-one relationship among matrices. Traffic-related emissions, wear of vehicle components, industrial contributions, mineral material, and redistribution of deposited particles may all contribute to this variability. The present data cannot establish the relative contribution of these sources.

4.3 Particle size influences

The particle-size analysis provides an additional explanation for some of the differences observed among the elements. Finer particles generally have greater specific surface area and may provide more surface for the association of certain PTEs. The observed relationships for Mn, Co, Cu, and particularly Ni are consistent with a role for particle-size distribution in determining PTE concentrations.

However, the relatively low explanatory power of many particle-size relationships indicates that grain size is not sufficient to explain PTE variability. The weak relationships observed for Cd, Cr, Pb, and Zn further demonstrate that their concentrations are influenced by additional factors. These may include mineralogical composition, source characteristics, atmospheric transport, deposition processes, and post-depositional redistribution.

The association of some PTEs with finer material is also consistent with previous studies reporting enrichment of certain metals in fine dust fractions (Sweeten et al., 1998; Kumar Yadav et al., 2025; Ahmady Birgani et al., 2017; Vlasov et al., 2022b; Lanzerstorfer, 2018). Nevertheless, the present results should not be used to infer direct source categories solely from particle size.

4.4 Potential geogenic and anthropogenic contributions

The combined statistical results indicate that both geogenic and anthropogenic contributions should be considered when interpreting the PTE patterns. In particular, Co and Cr should not be characterized exclusively as anthropogenic because both elements can occur naturally in soil and mineral dust. Their strong correspondence between DAD and DPAD may therefore reflect similar behavior of mineral-associated material as well as contributions from anthropogenic particulate matter.

Similarly, Ni should not be assigned exclusively to natural sources. Nickel may originate from mineral material but can also be associated with combustion and traffic-related activities, including petroleum-related emissions. Therefore, the present correlation and PCA results are more appropriately interpreted as indicating element groupings and correspondence rather than definitive source assignments.

The relatively high concentrations and asymmetric distributions observed for Cu, Pb, Zn, and Cd may be compatible with contributions from localized anthropogenic activities. However, asymmetry alone does not constitute proof of a nearby anthropogenic source. Traffic, industrial activities, combustion, atmospheric transport, mineral dust, and other mixed sources may contribute simultaneously.

The PCA grouping of Cd, Cu, Pb, Co, Cr, and Zn suggests that these elements share some common multivariate behavior in the present dataset, whereas Mn and Ni form a separate group. This pattern is consistent with the pairwise analyses but does not provide sufficient evidence for assigning the groups to a single source category. Thus, the present study should be considered an assessment of inter-matrix correspondence rather than a formal source-apportionment investigation.

4.5 Limitations of DPAD and SD as indicators of atmospheric deposition

Although DPAD showed strong correspondence with DAD for several elements, it should not be considered a universal substitute for direct atmospheric-deposition measurements. Leaf surfaces can retain deposited particles over time, but they may also be affected by washing, resuspension, particle retention characteristics, and other environmental processes.

Consequently, the concentration measured on leaves represents an integrated surface signal rather than an instantaneous measurement of atmospheric deposition.

Similarly, SD is subject to accumulation, resuspension, redistribution, and mixing of particles from different sources. These processes can weaken the correspondence between SD and newly deposited atmospheric material. The element-specific differences observed in this study are consistent with such complexity.

The present study was primarily designed to investigate correspondence among DAD, SD, and DPAD and was not designed as a comprehensive assessment of spatial or seasonal variability. Therefore, the observed relationships should not be assumed to be invariant across different locations or seasons. Dedicated multi-site and multi-season studies would be required to evaluate the stability and generalizability of these relationships under different meteorological and environmental conditions.

4.6 Monitoring implications

Despite these limitations, the findings indicate that DPAD may have practical value as a complementary, low-cost indicator for selected PTEs in atmospheric dust. In particular, the relatively strong correspondence observed for Zn, Cr, and Co suggests that DPAD can potentially retain useful information about the elemental composition of deposited atmospheric particles.

The results for SD indicate that it may also provide useful complementary information for selected elements, particularly where relatively strong inter-matrix correspondence is observed. However, its suitability is similarly element-dependent.

Overall, the findings support the concept of using DPAD and, for selected elements, SD as complementary monitoring matrices rather than as universal replacements for direct atmospheric-deposition sampling. Their application should be supported by site-specific validation and, where quantitative prediction is intended, independent measurements of atmospheric deposition.

5. Conclusions

This study evaluated the potential of street dust (SD) and dust deposited on date-palm leaves (DPAD) as complementary matrices for assessing the geochemical characteristics of deposited atmospheric dust (DAD) with respect to selected potentially toxic elements (PTEs). The results indicate that the degree of statistical correspondence among these three dust matrices is strongly element-dependent, suggesting that their potential complementary value for environmental monitoring varies among elements.

Mn exhibited weak and inconsistent relationships among the dust types, indicating that concentrations in SD or DPAD may not reliably reflect those in DAD for this element. Ni, Pb, Cu, and Cd showed dust-type-dependent relationships, with varying degrees of correspondence across the matrices. In contrast, Zn, Cr, and Co exhibited relatively strong relationships between DPAD and DAD, indicating closer correspondence for these elements within the sampled sites. However, these statistical relationships describe patterns in the present dataset and may not establish validated predictive performance beyond the study area.

DPAD, due to its cumulative nature and its ability to capture particles over extended time periods, may provide useful complementary information for assessing DAD-borne elements. This long-term accumulation reduces the influence of short-term meteorological fluctuations and effectively integrates the temporal average of the chemical composition of DAD. Nevertheless, DPAD was sampled only once, at the end of winter, whereas DAD was collected seasonally. Consequently, the observed relationships should not be interpreted as evidence of seasonally synchronized deposition or direct transfer from atmospheric dust to leaf surfaces. The extent to which DPAD represents atmospheric deposition may depend on environmental conditions, including rainfall, particle retention, and the duration of accumulation.

SD also showed relatively strong correspondence for selected elements, particularly Zn and Cu, suggesting that it may provide complementary information in some monitoring contexts. However, the strength of these relationships varied among elements. Differences in particle-size distribution, local inputs, resuspension, and the geochemical characteristics of street dust may contribute to the observed variability. Therefore, SD should not be considered a general substitute for direct atmospheric-deposition measurements. The multivariate analyses further supported the element-specific structure observed in the pairwise analyses. However, PCA and HCA did not provide definitive source apportionment, and the observed patterns may reflect combinations of geogenic and anthropogenic contributions, particle-size effects, atmospheric transport, and surface processes. In addition, the acid-extractable concentrations

761 measured using USEPA Method 3050B represent pseudo-total concentrations and do not
762 quantify the complete elemental inventory of silicate minerals. These methodological and
763 interpretive considerations should be taken into account when comparing the results with
764 studies using different digestion procedures.

765 Overall, DPAD and, for selected elements, SD may serve as useful complementary
766 information for environmental monitoring of atmospheric dust. However, their applicability is
767 element-dependent, and neither matrix should be regarded as a universal substitute for direct
768 atmospheric-deposition measurements. Further validation, particularly under different
769 environmental conditions and through dedicated multi-site and multi-season investigations,
770 would be necessary before the observed relationships are generalized or used for quantitative
771 prediction.

772

773 **Data Availability**

774 The datasets generated and/or analyzed during the current study are available from the
775 corresponding author upon reasonable request.

776 **References**

777 Adebiyi, A., et al. 2023. A review of coarse mineral dust in the Earth system. *Aeol. Res.* 60
778 100849. https://doi.org/10.1016/j.aeolia.2022.100849.

779 Akbari, Z., Kakuee, O., Shahbazi, R., Darvishi Khatooni, J. and Mashal, M. 2022. Assessment
780 of pollutant elements content in ambient air dust of Khuzestan Province. *J. Nucl. Res.*
781 *Appl.* 2(1), 45-60. https://sid.ir/paper/970339/en.

782

783 Ahmady Birgani, H., et al. 2017. Physico-chemical properties and mineralogical assessment of
784 aerosols and dust particles throughout the western Iran (case study: Abadan & Urmia
785 cities). *Journal of Range and Watershed Management,* 70 (3) , 551-567.
786 https://sid.ir/paper/162636/en. (In Persian).

787 Ahmed, M., et al. 2026. Heavy metals profiling of road dust from metro stations: spatial
788 distribution, source apportionment, and Monte Carlo simulation-based probabilistic
789 human health assessment. *Environ. Geochem. Health* 48 (203).
790 https://doi.org/10.1007/s10653-026-03094-y.

791 Al-Khashman, O. A., Al-Khashman, A. O., Hynes, N. R. J., Alnawafleh, H. M. and Velu, P. S.
792 2024. Assessment of heavy metals contamination of topsoil and street dust around

cement factory in southern Jordan. *J. Environ. Protec.* 15 (6), 672-696. https://doi.org/10.4236/jep.2024.156038.

Bierza, K. and Bierza, W. 2024. The effect of industrial and urban dust pollution on the ecophysiology and leaf element concentration of *Tilia cordata* Mill. *Environ. Sci. Pollut. Res*. 31, 58413–58429. https://doi.org/10.1007/s11356-024-34999-9.

Buljovčić, M., Živančev, Antić, I. and Đurišić-Mladenović, N., 2024. Heavy elements in indoor dust from Serbian households: pollution status, sources, and potential health risks. *Int. J. Environ. Health Res.* 34 (1), 50-60. https://doi.org/10.1080/09603123.2022.2128077.

Cai, K. and Li, C., 2019. Street dust heavy metal pollution source apportionment and sustainable management in a typical city _ Shijiazhuang, China. *Intern. J. Environ. Res. Public Health,* 16 (14), 2625. https://doi.org/10.3390/ijerph16142625.

Darvishi Khatooni, J., Vaezi, A. and Lak, R. 2026. Potentially toxic element contamination and ecological risk in surface sediments of the Khuzestan Plain, southwestern Iran: A province-wide geochemical baseline for a major Middle Eastern dust hotspot. *Soil Sed. Contam*. 1–35. https://doi.org/10.1080/15320383.2026.2692138.

Dehvari, M, Ramavandi, B., Maraghi, E., Ghaedrahmat, Z. and Ahmadi, M. 2025. Assessment of contamination status, source apportionment, and ecological and health risk of heavy metals in road dust: A case study in Masjed Soleyman City, Khuzestan, Iran. *Environ. Toxic.* 40(12):1387-1400. https://doi.org/10.1002/tox.24549.

Du, H., Lu, X. and Han, X. 2024. Spatial distribution characteristics and source apportionment of heavy metal(loid)s in park dust in the Mianyang urban area, China. *Environ. Geochem. Health* 46 (104). https://doi.org/10.1007/s10653-024-01901-y.

Ebrahimi Khusfi, Z., Khosroshahi, M., Roustaei, F. and Mirakbari, M. 2020. Spatial and seasonal variations of sand-dust events and their relation to atmospheric conditions and vegetation cover in semi-arid regions of central Iran. *Geoderma* 365, 114225. https://doi.org/10.1016/j.geoderma.2020.114225.

Esfandiari, M. and Hakimzadeh, M. A. 2022. Assessment of environmental pollution of heavy metals deposited on the leaves of trees at Yazd bus terminals. *Environ. Sci. Pollut. Res.* 29 (22), 32867-32881. https://doi.org/10.1007/s11356-021-18274-9.

Farmer, A. M. 1993. The effects of dust on vegetation—a review. *Environ. Pollut.* 79 (1), 63–75. https://doi.org/10.1016/0269-7491(93)90179-R.

Hossein Hamzeh, N. H., Kaskaoutis, D. G., Rashki, A. and Mohammadpour, K. 2021. Long-term variability of dust events in southwestern Iran and its relationship with the drought. *Atmosphere*, 12 (10), 1350. https://doi.org/10.3390/atmos12101350.

827 Heidari-Farsani, M., et al. 2013. The evaluation of heavy metals concentration related to PM_{10}
828 in ambient air of Ahvaz city, Iran. *J. Adv. Environ. Health Res.* 1(2), 120. http://
829 10.22102/jaehr.2013.40133.
830 Hojati, S., Khademi, H., Cano, A. and Landi, A. 2012. Characteristics of dust deposited along
831 a transect between central Iran and Zagros mountains. *Catena*, 88 (1), 27-36.
832 https://doi.org/10.1016/j.catena.2011.09.002.
833 IBM Corp. 2013. IBM SPSS statistics for Windows. Version 22.0. IBM Corp, Armonk, New
834 York.
835 Isinkaralar, O., Isinkaralar, K. and Ambade, B. 2024a. Assessment of societal health risks:
836 spatial distribution and potential hazards of toxic metals in street dust across diverse
837 communities. *Water Air Soil Pollut.* 235 (302), 1-17. https://doi.org/10.1007/s11270-
838 024-07104-6.
839 Isinkaralar, O., Isinkaralar, K. and Nguyen, T. N. T. 2024b. Spatial distribution, pollution level
840 and human health risk assessment of heavy metals in urban street dust at neighbourhood
841 scale. *Int. J. Biometeorol.* 68 (10), 2055-2067. https://doi.org/10.1007/s00484-024-
842 02729-y.

843 Islamic Republic of Iran Meteorological Organization (IRIMO). 2026. Meteorological data for
844 Khuzestan Province. https://www.irimo.ir/ (Accessed on Sept. 20, 2026).

845 Jish Prakash, P. et al. 2016. Arabian Red Sea coastal soils as potential mineral dust sources.
846 *Atmos. Chem. Phys.* 16 (18), 11991-12004. https://doi.org/10.5194/acp-16-11991-
847 2016.
848 Kabata-Pendias, A. and Mukherjee, AB. 2007. Trace Elements from Soil to Human. *Springer,*
849 B*erlin, Germany.* https://doi.org/10.1007/978-3-540-32714-1_19.
850
851 Karami, S., Hossein Hamzeh, N., Alam, K. and Ranjbar, A. 2020. The study of a rare frontal
852 dust storm with snow and rain fall: Model results and ground measurements. *J. Atmos.*
853 *Sol. Terr. Phys.* 197, 105149. https://doi.org/10.1016/j.jastp.2019.105149.
854 Karami, S., Kaskaoutis, D. G., Pytharoulis, I., Sotiropoulou, R. P. and Tagaris, E. 2024. Dust
855 transport from North Africa to the Middle East: synoptic patterns and numerical
856 forecast. *Atmosphere*, 15 (5), 531. https://doi.org/10.3390/atmos15050531.

857 Kumar Yadav , A., Gupta, K., Bodhale, R. and Phuleria, H. C. 2025. Metals and trace element
858 associated health risk in size-segregated household dust of an industrial town in India.
859 *Air Qual. Atmos. Health* 18, 2669–2685. https://doi.org/10.1007/s11869-025-01794-5.
860 Lanzerstorfer, C. 2018. Heavy metals in the finest size fractions of road-deposited sediments.
861 *Environ. Pollut.* 239, 522-531. https://doi.org/10.1016/j.envpol.2018.04.063.
862 Li, C. et al. 2021. Foliar dust as a reliable environmental monitor of heavy metal pollution in
863 comparison to plant leaves and soil in urban areas. *Chemosphere,* 287, 132341.
864 https://doi.org/10.1016/j.chemosphere.2021.132341.
865 Liao, S. et al. 2021. The quantitative source apportionment of heavy metals in peri-urban
866 agricultural soils with UNMIX and input fluxes analysis. *Environ. Technol. Innov.* 21,
867 101232, https://doi.org/10.1016/j.eti.2020.101232.
868 Liu, Y., Dong, J., Zhang, N. and Wang, H. 2025. Characteristics, source apportionment, and
869 health risk assessment of pollution of heavy metals in plant foliar dust: characterization
870 of atmospheric heavy metal pollution. *Environ. Geochem. Health* 47 (361).
871 https://doi.org/10.1007/s10653-025-02660-0.
872 Lu, X., Wang, L., Li, L.Y., Lei, K., Huang, L. and Kang, D. 2010. Multivariate statistical
873 analysis of heavy metals in street dust of Baoji, NW China. *J. Hazardous Mat.* 173 (1-
874 3), 744-749. https://doi.org/10.1016/j.jhazmat.2009.09.001.
875 Łukowski, A., Popek, R. and Karolewski, P. 2020. Particulate matter on foliage of *Betula*
876 *pendula*, *Quercus robur*, and *Tilia cordata*: deposition and ecophysiology. *Environ.*
877 *Sci. Pollut. Res.* 27 (10), 10296-10307. https://doi.org/10.1007/s11356-020-07672-0.
878 MalAmiri, N., Rashki, A., Hosseinzadeh, S. R. and Kaskaoutis, DG. 2022. Mineralogical,
879 geochemical, and textural characteristics of soil and airborne samples during dust
880 storms in Khuzestan, southwest Iran. *Chemosphere* 286, 131879.
881 https://doi.org/10.1016/j.chemosphere.2021.131879.
882 McTainsh, G.H., Nickling, W.G. and Lynch, A.W. 1997. Dust deposition and particle size in
883 Mali, West Africa. *Catena* 29, 307–322. https://doi.org/10.1016/S0341-
884 8162(96)00075-6.
885 Mostafaii, G. et al. 2021. Health risk assessment and source apportionment of heavy metals in
886 atmospheric dustfall in a city of Khuzestan Province, Iran. *J. Environ. Health Sci.*
887 *Eng.* 19, 585–601. https://doi.org/10.1007/s40201-021-00630-z.
888 Naderizadeh, Z., Khademi, H. and Ayoubi, S. 2016. Biomonitoring of atmospheric heavy
889 metals pollution using dust deposited on date palm leaves in southwestern Iran.
890 *Atmósfera* 29 (2), 141-155. https://doi.org/10.20937/ATM.2016.29.02.04.

Najmeddin, A., Keshavarzi, B., Moore, F. and Lahijanzadeh, A. 2017. Source apportionment and health risk assessment of potentially toxic elements in road dust from urban industrial areas of Ahvaz megacity, Iran. *Environ. Geochem. Health*, 40, 1187–1208. https://doi.org/10.1007/s10653-017-0035-2.

Naraki, H., Keshavarzi, B., Zarei, M., Moore, F., Abbasi, S., Kelly, F.J., Dominguez, A. O. and Jaafarzadeh, N. 2021. Urban street dust in the Middle East oldest oil refinery zone: Oxidative potential, source apportionment and health risk assessment of potentially toxic elements. *Chemosphere*, 268, 128825. https://doi:10.1016/j.chemosphere.2020.128825.

Niu, S., Song, X., Yu, J., Wang, X. and Liana, J. 2020. Particle size dependent heavy metals in road dusts from maanshan city, china. *KSCE J. Civ. Eng.* 24 (5), 1411-1423. https://doi.org/10.1007/s12205-020-2193-5.

Norouzi, S. and Khademi, H. 2015. Spatial and temporal variation in dust deposition rate in Isfahan and its relationship with selected climatic parameters. *J. Soil Water Sci.* 19 (72), 149-162. https://doi.org/10.18869/acadpub.jstnar.19.72.14 (In Persian with an English abstract).

Öncü, T., Yazman, M. M., Ustaoğlu, F., Hristova, E. and Yüksel, B. 2025. Source dynamics and environmental risk of street dust as a vector of human exposure to potentially toxic elements in Istanbul, Türkiye. *Sci. Rep.* 15 (1), 30550. https://doi.org/10.1038/s41598-025-11472-2.

Parno, R. et al. 2024. Investigating the role of the low-level jet in two winters severe dust rising in Southwest Iran. *Atmosphere* 15 (4), 400. https://doi.org/10.3390/atmos15040400.

Pourfadakari, S., Jorfi, S., Ravanbakhash, M., Talepour, N. and Karimian, R. 2024. Determination of geochemical baselines and evaluation of potentially toxic elements in agricultural soils of Ramhormoz Plain, Iran. *Int. J. Environ. Health Res.* 34 (8), 3011–3024. https://doi.org/10.1080/09603123.2023.2283060.

Pourret, O. and Hursthouse, A. 2019. It's time to replace the term "heavy metals" with "potentially toxic elements" when reporting environmental research. *Int. J. Environ. Res. Public Health* 16 (4446), 1-6. https://doi.org/10.3390/ijerph16224446.

Proestakis, E. et al. 2025. Atmospheric dust and air quality over large-cities and megacities of the World. *EGUsphere* 25 (21), 14777 – 14823. https://doi.org/10.5194/acp-25-14777-2025.

924 Qiu, Y., Guan, D., Song, W. and Huang, K. 2009. Capture of heavy metals and sulfur by foliar
925 dust in urban Huizhou, Guangdong Province, China. *Chemosphere* 75 (4), 447-452.
926 https://doi.org/10.1016/j.chemosphere.2008.12.061.
927 Rana, M. S., Wang, Q., Wang, W., Enyoh, C.E., Islam, M. R., Isobe, Y. and Kabir, M. H. 2024.
928 Sources, distribution, and health implications of heavy metals in street dust across
929 industrial, capital city, and peri-urban areas of Bangladesh. *Atmosphere* 15 (9), 1088.
930 https://doi.org/10.3390/atmos15091088.
931 Rehman, A. et al. 2025. Unveiling sources, contamination, and eco-human health implications
932 of potentially toxic metals from urban road dust. *Sci. Rep.* 15 (1), 10673.
933 https://doi.org/10.1038/s41598-025-95205-5.
934 Sabetghadam, S., Alizadeh, O., Khoshsima, M. and Pierleoni, A. 2021. Aerosol properties,
935 trends and classification of key types over the Middle East from satellite-derived
936 atmospheric optical data. *Atmos. Environ.* 246, 118100.
937 https://doi.org/10.1016/j.atmosenv.2020.118100.
938 Sadeghdoust, F., Ghanavati, N., Nazarpour, A., Babaenejad, T. and James Watts, M. 2020.
939 Hazard, ecological, and human health risk assessment of heavy metals in street dust in
940 Dezful, Iran. *Arab. J. Geosci.* 13 (17), 881. https://doi.org/10.1007/s12517-020-05915-
941 5.
942 Salmabadi, H., Saeedi, M., Roy, A. and Kaskaoutis, D. G. 2023, Quantifying the contribution
943 of Middle Eastern dust sources to PM_{10} levels in Ahvaz, Southwest Iran. *Atmos. Res.*
944 295, 106993. https://doi.org/10.1016/j.atmosres.2023.106993.
945 Semerjian, L. et al. 2021. Global systematic mapping of road dust research from 1906 to 2020:
946 Research gaps and future direction. *Sustainability* 13, 11516.
947 https://doi.org/10.3390/su132011516.
948 Shao, Y. et al. 2011. Dust cycle: An emerging core theme in Earth system science. *Aeol. Res.*
949 2 (4), 181-204. https://doi.org/10.1016/j.aeolia.2011.02.001.
950 Singh, H., Singh, P., Agrawal, S. B. and Agrawal, M. 2022. Implications of foliar particulate
951 matter deposition on the physiology and nutrient allocation of dominant perennial
952 species of the Indo-Gangetic Plains. *Front. Plant Sci.* 13, 1-13. https://
953 doi.org/10.3389/fpls.2022.939950.
954 Soliman, H. A. et al. 2025. Assessment of heavy metals in total suspended particles and
955 deposited dust in different areas in Assiut city, Egypt. *Sci. Rep.* 15 (1), 32574.
956 https://doi.org/10.1038/s41598-025-18697-1.

957 Statistical Center of Iran. 2025. Website of the Statistical Center of Iran. [online] Available at:
958 https://www.amar.org.ir [Accessed on 12 November 2025].
959 Su, C., Zhao, W., Dong, J., Zhong, Y. X. and Yang, Z. Q. 2026. Vertical distribution
960 characteristics and source analysis of heavy metals in near-surface urban dust in Central
961 Beijing. *Environ. Geochem. Health* 48 (257). https://doi.org/10.1007/s10653-026-
962 03154-3.
963 Sweeten, J. M., Parnell, Jr. CB., Shaw, B.W. and Auvermann, B. W. 1998. Particle size
964 distribution of cattle feedlot dust emission. *Trans. ASAE* 41 (5), 1477-1481.
965 U.S. Environmental Protection Agency (USEPA). 1996. Method 3050B: Acid Digestion of
966 Sediments, Sludges, and Soils. Revision 2. Washington, DC: U.S. EPA.
967 https://www.epa.gov/sites/default/files/2015-06/documents/epa-3050b.
968 Taghipour, M., Ayoubi, S. and Khademi, H. 2011. Contribution of lithologic and
969 anthropogenic factors to surface soil heavy metals in western Iran using multivariate
970 geostatistical analyses. *Soil Sediment Contam*. 20 (8), 921-937.
971 https://doi.org/10.1080/15320383.2011.620045. Tan, S. Y., Praveena, S. M., Emilia, Z.
972 C. and Manraj S. 2016. A review of heavy metals in indoor dust and its human health-
973 risk implications. *Rev. Environ. Health* 31 (4), 447-456. https://doi.org/10.1515/reveh-
974 2016-0026.
975 Vaezi, A., Shahbazi, R., Lak, R., Ahmadi, N., Sheikh, M. and Mohammadi,
976 A.R. 2023. Assessment of potentially toxic elements in atmospheric dust and
977 associated health risks in Zahedan City, Iran. *Environ. Geochem. Health* 45, 7759–
978 7773. https://doi.org/10.1007/s10653-023-01674-w.
979 Vaezi, A., Shahbazi, R., Sheikh, M., Lak, R., Ahmadi, N., Kaskaoutis, D.G., Dahmardeh
980 Behrooz, R., Sotiropoulou, R.E.P. and Targaris, E. 2024. Environmental pollution and
981 human health risks associated with atmospheric dust in Zabol City, Iran. *Air Qual.*
982 *Atmos. Health* 17, 2491–2513. https://doi.org/10.1007/s11869-024-01582-7.
983 Vlasov, D. V., Ramírez, O. and Luhar, A. 2022a. Road dust in urban and industrial
984 environments: sources, pollutants, impacts, and management. *Atmosphere* 13 (4), 607.
985 http;// doi.org/10.3390/atmos13040607.
986 Vlasov, D. V., Kukushkina, O. V., Kosheleva, N. E. and Kasimov, N. S. 2022b. Levels and
987 factors of the accumulation of metals and metalloids in roadside soils, road dust, and
988 their PM_{10} fraction in the western Okrug of Moscow. *Eurasian Soil Sc*i. 55, 556–572.
989 https://doi.org/10.1134/S1064229322050118.

Wang, J. et al. 2020. Contamination, morphological status and sources of atmospheric dust in different land-using areas of a steel-industry city, China. *Atmos. Pollut. Res.* 11 (2), 283-289. https://doi.org/10.1016/j.apr.2019.10.014.

Williams, M. 2012. Manganese in air: Environmental sources, transport, and health implications. *National Center for Biotechnology Information.* Available at: https://www.ncbi.nlm.nih.gov/books/NBK158869/.

Xia, B. et el. 2025. Identifying hidden heavy metal sources in atmospheric dust of mining cities by integrating Cd isotopes and multivariate statistical method. *J. Hazard. Mater.* 45 (138894), https://doi.org/10.1016/j.jhazmat.2025.138894.

Yousefi-Kebriya, A., Nadi, M., Afaridegan, E. and Sun, Z. 2025. Wetland shrinking and dust pollution in Khuzestan Iran: insights from sentinel-5 and MODIS satellites. *Sci. Rep.* 15 (1), 13626. https://doi.org/10.1038/s41598-025-96935-2.

Zhao, P., Liu, X., Yin, L., Tian, D. and Wang, X. 2022. Levels, distribution characteristics, and sources of heavy metals in indoor dust in Shijiazhuang, China. *Environ. Monit. Assess.* 194 (12), 857. https://doi.org/10.1007/s10661-022-10543-5.

Declarations

Funding

This research was financially supported by Isfahan University of Technology (IUT), Isfahan, Iran.

Consent for publication

Not applicable, as this investigation did not involve human participants, human data, or personal information.

Competing interests

The authors declare that they have no known competing financial interest or personal relationships that could have appeared to influence the work reported in this paper.

Table 1. Number of various types of dust samples collected from different cities of Khuzestan Province

Cities	Atmospheric dust (DAD)	Street dust (SD)	Date palm-associated dust (DPAD)
Abadan	4	4	4
Khorramshahr	3	3	3
Shadegan	2	2	2
Ahvaz And Hamidieh	7	7	7
Karoon	2	2	2
Bavi	2	2	2
Shushtar and Gotvand	4	4	4
Shush and Karkheh	3	3	3
Dezful	5	5	5
Total each season	32	32	32
Total per year	128	128	32

1022 Table 2. Descriptive statistics of PTE concentrations (mg kg^{-1}) in different types of dust including deposited
1023 atmospheric dust (DAD), street dust (SD), and date palm-associated dust (DPAD) (N=32).

Element	Dust type	Min.	Max.	Range	Mean	Median	Mode	SD	Var.	CV (%)	SK	Kurt
Mn	DAD	1208.1	2163.1	955.0	1651.5	1668.9	1208.1	233.4	54516.8	14.1	0.1	-0.4
	SD	750.9	1974.0	1223.1	1250.4	1169.6	750.9	300.3	90207.2	24.0	0.7	0.2
	DPAD	727.5	2441.2	1713.7	1522.2	1458.7	1686.2	325.0	105647.0	21.4	0.5	1.5
Cd	DAD	0.3	1.6	1.3	0.5	0.5	0.6	0.2	0.0	41.9	3.8	18.0
	SD	0.3	2.5	2.1	0.5	0.5	0.3	0.3	0.1	64.0	4.6	24.2
	DPAD	0.3	2.4	2.0	0.6	0.5	0.3	0.3	0.1	59.3	4.0	19.7
Co	DAD	30.8	70.2	39.3	38.8	37.4	30.8	7.7	60.0	20.0	2.8	9.3
	SD	20.5	60.4	39.8	31.5	30.3	20.5	7.6	58.3	24.2	2.1	6.4
	DPAD	28.5	68.4	39.9	38.0	35.7	34.0	7.9	63.7	21.0	2.6	7.5
Cr	DAD	40.5	100.2	59.7	65.4	67.8	69.0	12.9	167.8	19.8	0.2	0.3
	SD	37.2	101.5	64.2	54.6	51.2	47.5	12.7	161.6	23.3	1.6	4.7
	DPAD	38.0	102.0	64.0	63.3	67.5	68.0	13.5	183.0	21.4	0.2	1.0
Cu	DAD	37.6	948.2	910.6	120.2	77.9	37.6	159.1	25314.5	132.3	4.8	25.4
	SD	22.4	375.5	353.0	71.1	50.8	22.4	63.9	4092.5	89.9	3.7	16.9
	DPAD	33.4	746.0	712.6	106.9	76.7	33.4	124.3	15460.1	116.3	4.6	24.0
Ni	DAD	39.9	86.7	46.7	61.6	61.3	39.9	11.0	121.6	17.9	0.1	-0.3
	SD	19.1	74.8	55.6	41.7	38.7	19.1	13.5	182.7	32.4	0.6	-0.0
	DPAD	40.8	78.7	37.9	58.8	58.9	40.8	9.9	98.5	16.9	0.1	-0.6
Pb	DAD	67.9	298.6	230.6	136.6	127.8	67.9	50.1	2512.7	36.7	1.2	2.4
	SD	45.2	408.7	363.5	110.2	105.2	45.2	61.9	3841.8	56.2	3.7	17.9
	DPAD	60.6	469.1	408.4	139.8	131.7	60.6	70.1	4918.3	50.2	3.4	15.9
Zn	DAD	106.5	694.7	588.1	305.6	258.6	106.5	180.3	32533.9	59.0	0.6	-0.8
	SD	63.1	452.4	389.2	231.8	224.2	63.1	125.3	15705.8	54.1	0.3	-1.1
	DPAD	70.7	845.4	774.7	297.6	208.6	70.7	209.5	43903.1	70.4	1.2	0.6

Min: Minimum; Max: Maximum; SD: Standard deviation; CV: Coefficient of variation; SK: Skewness; Kurt: Kurtosis

1024 =Table 3. Pairwise correlation coefficients of elemental concentrations among three types of
1025 dust

Element	Dust type pair	N (Outlier removed)	Correlation coefficient	Test	p-value	Significance
Mn	DAD – SD	30	-0.229	Pearson	0.224	ns
	DAD - DPAD	30	-0.300	Spearman	0.108	ns
	SD - DPAD	30	0.037	Spearman	0.845	ns
Cd	DAD – SD	30	0.526	Pearson	0.003	**
	DAD - DPAD	30	0.187	Spearman	0.322	ns
	SD - DPAD	30	0.761	Spearman	<0.001	***
Co	DAD – SD	29	0.213	Pearson	0.267	ns
	DAD - DPAD	29	0.831	Pearson	<0.001	***
	SD - DPAD	29	0.305	Pearson	0.108	ns
	DAD – SD	31	0.326	Pearson	0.073	ns

Cr	DAD - DPAD	31	0.888	Spearman	<0.001	***
	SD - DPAD	31	0.307	Spearman	0.094	ns
Cu	DAD – SD	28	0.494	Spearman	0.008	**
	DAD - DPAD	28	0.524	Spearman	0.004	**
	SD - DPAD	28	0.700	Spearman	<0.001	***
Ni	DAD – SD	31	0.537	Pearson	0.002	**
	DAD - DPAD	31	0.423	Pearson	0.018	*
	SD - DPAD	31	0.183	Pearson	0.326	ns
Pb	DAD – SD	31	0.359	Pearson	0.047	*
	DAD - DPAD	31	0.532	Pearson	0.002	**
	SD - DPAD	31	0.277	Pearson	0.132	ns
Zn	DAD – SD	29	0.655	Spearman	<0.001	***
	DAD - DPAD	29	0.720	Spearman	<0.001	***
	SD - DPAD	29	0.625	Spearman	<0.001	***

- DAD: Deposited atmospheric dust; SD: Street dust; DPAD: Date palm associated dust
- Pearson correlation was applied to normally distributed data, while Spearman rank correlation was used for non-normally distributed variables.
- ns: non-significant; * p-value < 0.05; ** p-value < 0.01; *** p-value < 0.001

1028 Table 4. Pairwise linear regression statistics and residual diagnostics for PTE concentrations among
1029 deposited atmospheric dust (DAD), street dust (SD), and date palm-associated dust (DPAD)

Element	Dust type pair	N	Slope (B_1)	SE (B_1)	Intercept (B_0)	R^2	p-value	Std. residual range
Mn	DAD – SD	30	-0.301	0.243	1738.953	0.052	0.224 ^{ns}	-1.410 to 2.121
	DAD - DPAD	30	-0.348	0.192	2087.889	0.105	0.080 ^{ns}	-1.811 to 2.118
	SD - DPAD	30	0.077	0.153	1421.894	0.009	0.617 ^{ns}	-1.242 to 2.204
Cd	DAD – SD	30	0.603	0.184	0.202	0.277	0.003 **	-1.847 to 1.922
	DAD - DPAD	30	0.435	0.253	0.032	0.095	0.097 ^{ns}	-1.801 to 2.250
	SD - DPAD	30	1.011	0.132	0.026	0.676	< 0.001 ***	-1.844 to 2.888
Co	DAD – SD	29	0.296	0.261	18.899	0.045	0.267 ^{ns}	-1.877 to 2.418
	DAD - DPAD	29	0.854	0.110	4.502	0.691	< 0.001 ***	-1.902 to 1.888
	SD - DPAD	29	0.225	0.135	29.146	0.093	0.108 ^{ns}	-2.039 to 2.561
Cr	DAD – SD	31	0.271	0.146	35.629	0.106	0.073 ^{ns}	-1.943 to 2.186
	DAD - DPAD	31	0.962	0.064	0.233	0.885	< 0.001 ***	-2.061 to 2.090
	SD - DPAD	31	0.453	0.212	38.052	0.136	0.041 *	-2.087 to 1.801
Cu	DAD – SD	28	0.245	0.136	35.115	0.111	0.084 ^{ns}	-1.116 to 3.409
	DAD - DPAD	28	0.352	0.159	47.504	0.159	0.036 *	-1.538 to 2.772
	SD - DPAD	28	0.911	0.153	26.363	0.577	< 0.001 ***	-1.729 to 2.643
Ni	DAD – SD	31	0.612	0.179	3.228	0.284	0.002 **	-1.743 to 1.903
	DAD - DPAD	31	0.395	0.157	34.639	0.179	0.018 *	-2.161 to 1.796
	SD - DPAD	31	0.150	0.150	52.716	0.033	0.326 ^{ns}	-2.013 to 1.871
Pb	DAD – SD	31	0.262	0.127	66.145	0.129	0.047 *	-1.747 to 2.305
	DAD - DPAD	31	0.475	0.140	66.705	0.283	0.002 **	-1.603 to 1.964
	SD - DPAD	31	0.338	0.218	95.118	0.077	0.132 ^{ns}	-2.015 to 1.735
Zn	DAD – SD	29	0.544	0.112	67.793	0.465	< 0.001 ***	-1.381 to 2.084
	DAD - DPAD	29	0.809	0.109	29.596	0.673	< 0.001 ***	-2.099 to 2.606
	SD - DPAD	29	0.736	0.191	90.443	0.354	< 0.001 ***	-1.638 to 3.208

- DAD: Deposited atmospheric dust; SD: Street dust; DPAD: Date palm associated dust**;** N: number of observations included in the regression analysis after outlier removal; B_1: unstandardized regression slope coefficient; SE: standard error of B_1; B_0: regression intercept (constant); R^2: coefficient of determination; p-value: significance level of the regression model; Std. residual range: minimum and maximum standardized regression residuals**;** ns: non-significant; * p-value < 0.05; ** p-value < 0.01; *** p-value < 0.001

1030

1031

1032 Table 5. Total variance explained by principal component analysis of PTE concentrations in
1033 the three dust types

Component	Initial Eigenvalues			Rotation sums of squared loadings		
	Total	% of Variance	Cumulative %	Total	% of Variance	Cumulative %
1	4.341	54.261	54.261	3.836	47.953	47.953
2	1.390	17.381	71.642	1.895	23.689	71.642
3	0.763	9.543	81.185			
4	0.517	6.458	87.643			
5	0.425	5.312	92.955			
6	0.256	3.195	96.150			
7	0.173	2.166	98.316			
8	0.135	1.684	100.000			

1034

1035

Table 6. Varimax-rotated component loadings and communalities of PTEs

PTEs	PC1	PC2	Communality
Cd	0.899	0.056	0.811
Cu	0.871	0.132	0.776
Pb	0.824	0.085	0.686
Co	0.771	0.471	0.815
Cr	0.717	0.416	0.686
Zn	0.637	0.028	0.407
Mn	−0.040	0.875	0.767
Ni	0.276	0.841	0.783
Variance (%)	47.953	23.689	
Cumulative variance (%)	47.953	71.642	

Table 7. Statistical comparison of PCA scores among the three dust types

PC	Friedman χ^2	P_Value	DAD–DPAD	DAD–SD	DPAD–SD
PC1	13.000	0.002	0.411 ^{ns}	0.006*	0.002*
PC2	35.688	<0.001	0.020 ^{ns}	<0.001*	<0.001*

Ns: non-significant after Bonferroni correction; * significant after Bonferroni correction (adjusted $\alpha = 0.0167$).

1046
1047
1048
1049 Table 8. Particle size distribution statistics of dust samples (%)

		Clay	Fine silt	Coarse silt	Very fine sand	Fine sand	Medium sand	Coarse sand	Very coarse sand	Equivalent diameter less than		
										2.5µm	5µm	10 µm
DAD (n =18)	Min	3.3	39.1	1.3	0.0	0.0	0.0	0.0	0.0	4.1	11.4	26.5
	Max	25.0	85.3	45.2	19.0	10.0	0.2	0.1	0.0	28.5	51.3	80.1
	Mean	14.1	64.6	16.9	3.7	0.6	0.0	0.0	0.0	16.5	31.5	53.2
	SD	5.6	12.1	10.5	5.2	1.9	0.0	0.0	0.0	6.3	10.0	14.6
SD (n =11)	Min	0.3	11.9	6.7	0.7	0.2	0.0	0.0	0.0	0.8	2.5	8.7
	Max	37.8	74.9	31.1	32.4	32.8	14.7	0.5	0.0	40.0	48.8	66.6
	Mean	6.9	35.8	18.3	18.5	16.3	4.1	0.1	0.0	8.5	16.6	28.1
	SD	9.5	15.7	7.1	7.7	8.0	4.2	0.2	0.0	9.8	11.4	13.6
DPAD (n =30)	Min	5.1	33.0	0.1	0.0	0.0	0.0	0.0	0.0	5.9	12.0	22.1
	Max	33.5	90.7	22.6	9.0	18.2	15.0	1.0	0.0	40.8	78.9	98.9
	Mean	14.8	69.5	13.0	1.4	0.8	0.5	0.0	0.0	17.4	33.3	55.7
	SD	6.6	9.5	6.7	2.2	3.4	2.7	0.2	0.0	7.5	12.7	14.4

- DAD: Deposited atmospheric dust; SD: Street dust; DPAD: Date palm associated dust
- Min: Minimum; Max: Maximum; SD: Standard deviation

1050
1051
1052

Table 9. Correlation coefficients between element concentrations and particle size distribution across different dust types

Element	Size fraction (%)	Correlation coefficient	Test	Significance	R^2
Mn	Clay	0.145	Pearson	ns	0.021
	Silt	0.446	Pearson	**	0.2
	Sand	-0.434	Pearson	**	0.2
	Clay + fine Silt	0.368	Pearson	**	0.13
	Coarse Silt + Sand	-0.368	Pearson	**	0.13
Cd	Clay	0.075	Spearman	ns	0.01
	Silt	0.007	Spearman	ns	0.01
	Sand	-0.141	Spearman	ns	0.02
	Clay + fine Silt	0.121	Spearman	ns	0.01
	Coarse Silt + Sand	-0.121	Spearman	ns	0.01
Co	Clay	0.373	Spearman	**	0.13
	Silt	0.090	Spearman	ns	0.08
	Sand	-0.377	Spearman	**	0.16
	Clay + fine Silt	0.469	Spearman	***	0.15
	coarse Silt + Sand	-0.469	Spearman	***	0.15
Cr	Clay	0.097	Pearson	ns	0.01
	Silt	0.224	Pearson	ns	0.05
	Sand	-0.228	Pearson	ns	0.05
	Clay + fine Silt	0.142	Pearson	ns	0.02
	Coarse Silt + Sand	-0.142	Pearson	ns	0.02
Cu	Clay	0.336	Spearman	*	0.04
	Silt	-0.071	Spearman	ns	0.01
	Sand	-0.299	Spearman	*	0.03
	Clay + fine Silt	0.410	Spearman	**	0.03
	Coarse Silt + Sand	-0.410	Spearman	**	0.03
Ni	Clay	0.368	Pearson	**	0.13
	Silt	0.485	Pearson	***	0.23
	Sand	-0.562	Pearson	***	0.32
	Clay + fine Silt	0.568	Pearson	***	0.32
	Coarse Silt + Sand	-0.568	Pearson	***	0.32
Pb	Clay	0.048	Spearman	ns	0.001
	Silt	0.299	Spearman	*	0.05
	Sand	-0.175	Spearman	ns	0.04
	Clay + fine Silt	0.235	Spearman	ns	0.04
	Coarse Silt + Sand	-0.235	Spearman	ns	0.04
Zn	Clay	0.017	Spearman	ns	0.02
	Silt	0.107	Spearman	ns	0.03
	Sand	-0.033	Spearman	ns	0.04
	Clay + fine Silt	-0.043	Spearman	ns	0.02
	Coarse Silt + Sand	0.043	Spearman	ns	0.02

- Pearson correlation was applied to normally distributed data, while Spearman rank correlation was used for non-normally distributed variables.
- ns: non-significant; * p-value < 0.05; ** p-value < 0.01; *** p-value < 0.001

Table 10. Comparison of PTE concentrations (mg kg^{-1}) in different dust types and surface soils reported for Khuzestan and neighboring regions with those obtained in the present study

City/Province	Dust type/ Soil	Mn	Cd	Co	Cr	Cu	Ni	Pb	Zn	References
Dezful	DAD	ND	1.2	ND	393.5	ND	320.1	45.1	ND	(Mostafaii et al., 2021)
Abadan	DAD	564.3	ND	ND	134.2	ND	ND	ND	196.1	(Akbari et al., 2022)
Bushehr	DPAD	365.1	ND	11.7	35.7	54.0	79.0	68.0	170.0	(Naderizadeh et al., 2016)
Dezful	SD	ND	0.4	8.0	44.0	51.0	46.0	54.0	224.0	(Sadeghdoust et al., 2020)
Ahvaz	SD	564.6	0.5	9.8	51.5	74.4	59.7	85.5	308.9	(Najmeddin et al., 2017)
Abadan	SD	ND	1.2	ND	ND	83.6	ND	49.8	281.2	(Naraki et al., 2021)
Khorramshahr	SD	ND	0.6	ND	ND	74.3	ND	56.5	214.3	(Naraki et al., 2021)
Khuzestan	SS	478.0	0.6	25.0	65.0	20.0	115.0	20.0	49.0	(Darvishi Khatooni et al., 2026)
Ramhormoz	SS	217.0	0.6	ND	60.0	10.6	23.0	3.6	14.0	(Pourfadakari et al., 2024)
World soil average	SS	418.0	1.1	6.9	59.5	23.7	28.0	25.0	62.0	(Kabata-Pendias and Mukherjee, 2007)
Khuzestan	DAD	1651.6	0.6	38.8	64.4	120.2	61.7	136.7	305.7	Current study
	DPAD	1522.3	0.6	38.1	63.3	106.9	58.9	139.8	297.7	
	SD	1250.5	0.6	31.6	54.6	71.1	41.7	110.3	231.8	
	SS	248.0	0.1	9.6	23.5	19.4	18.3	14.4	29.7	

ND: Not determined, DAD: Deposited atmospheric dust, SD: street dust, DPAD: Date palm-associated dust, SS: Surface soil

Figure captions

Fig. 1. Geographic location of the study area showing the sampling sites in selected cities of Khuzestan Province, southwestern Iran, and its position within Iran and the world. The map was prepared by the authors using ArcGIS Desktop (ArcMap), version 10.8.2 (Esri; https://desktop.arcgis.com/en/arcmap/latest/). Administrative boundary data were obtained from OpenStreetMap via Geofabrik (https://download.geofabrik.de/). Map data © OpenStreetMap contributors, available under the Open Database License (ODbL; https://www.openstreetmap.org/copyright). Sampling locations were plotted using geographic coordinates recorded in the field.

Fig. 2. Photo of a ceramic atmospheric dust trap designed and installed on the roof. The photograph was taken by the first author during field sampling.

Fig. 3. Mean metal concentrations in DAD (atmospheric dust), SD (street dust) and DPAD (Date palm associated dust) as compared to 3 different thresholds for soil including USEPA ecological threshold (R1), The Netherlands soil guideline (R2), and local background soil based on the analysis carried out in this study (R3). Different letters indicate significant difference at 0.05 probability level based on the LSD test. Bars denote standard errors of the means.

Fig. 4. Linear regression of elemental concentrations (mg kg^{-1}) among different types of dust including atmospheric dust (DAD), street dust (SD), and date palm-associated dust (DPAD).

Fig. 5. Varimax-rotated PCA loading plot of the eight potentially toxic elements in DAD, SD and DPAD.

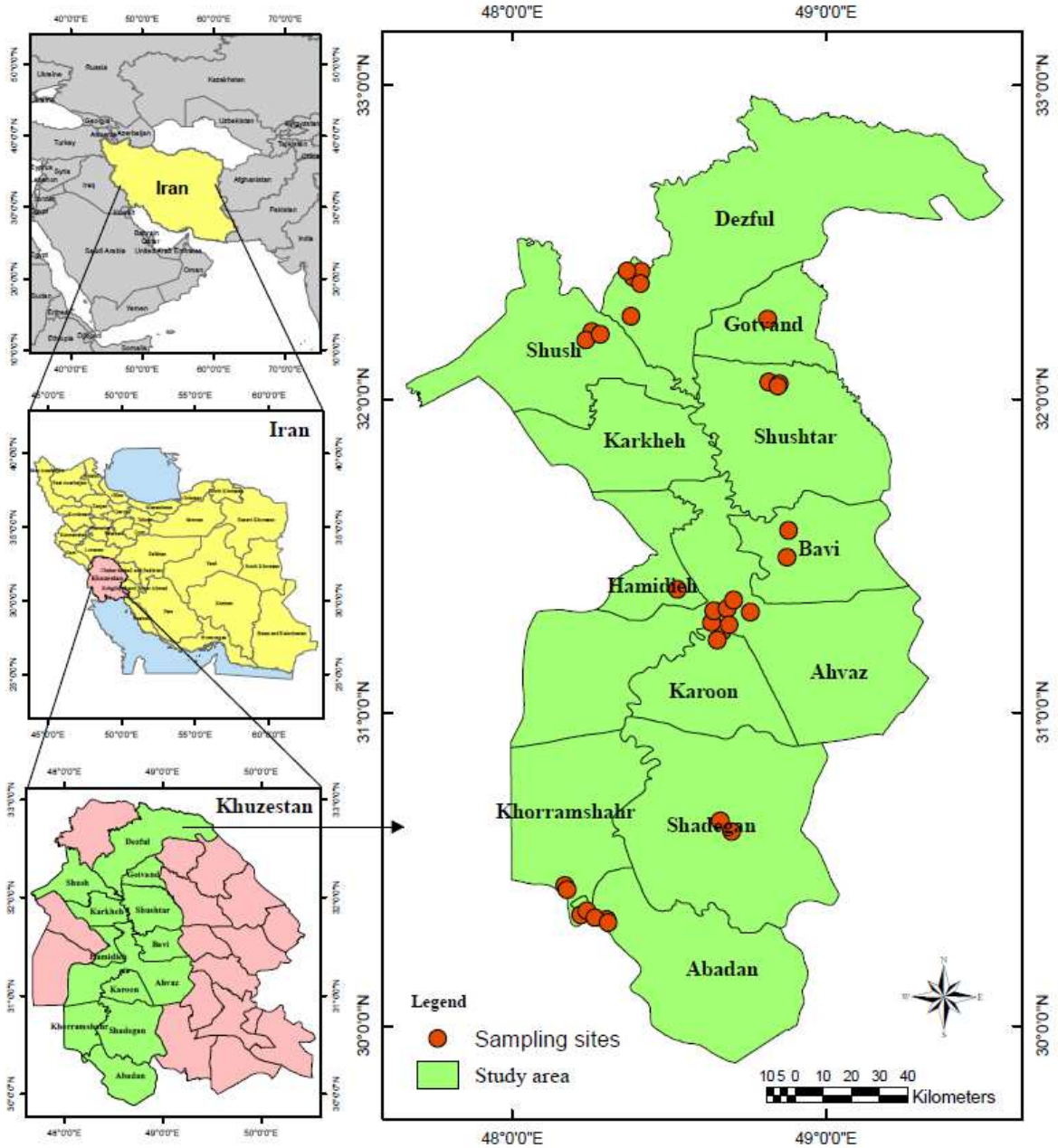
Fig. 6. PCA score plot of deposited atmospheric dust (DAD), street dust (SD), and date palm-associated dust (DPAD) based on the concentrations of eight potentially toxic elements. PC1 and PC2 accounted for 47.95% and 23.69% of the total variance, respectively.

Fig. 7. Dendrogram of hierarchical cluster analysis of the eight potentially toxic elements using Ward's linkage method.

Fig. 8. Particle size distribution (%) in different types of dust including deposited atmospheric dust (DAD), street dust (SD), and date palm associated dust (DPAD).

Fig. 9. Conceptual summary of the observed relationships among potentially toxic elements (PTEs) in deposited atmospheric dust (DAD), street dust (SD), and date palm-associated dust (DPAD), based on the results of the present study. The figure was created by the authors using Adobe Photoshop 2026, version 27.10 (Adobe Inc., San Jose, CA, USA; https://helpx.adobe.com/photoshop/desktop/whats-new/whats-new-in-adobe-photoshop-on-desktop.html).

1111
1112
1113



1114
1115

Fig. 1



Fig. 2

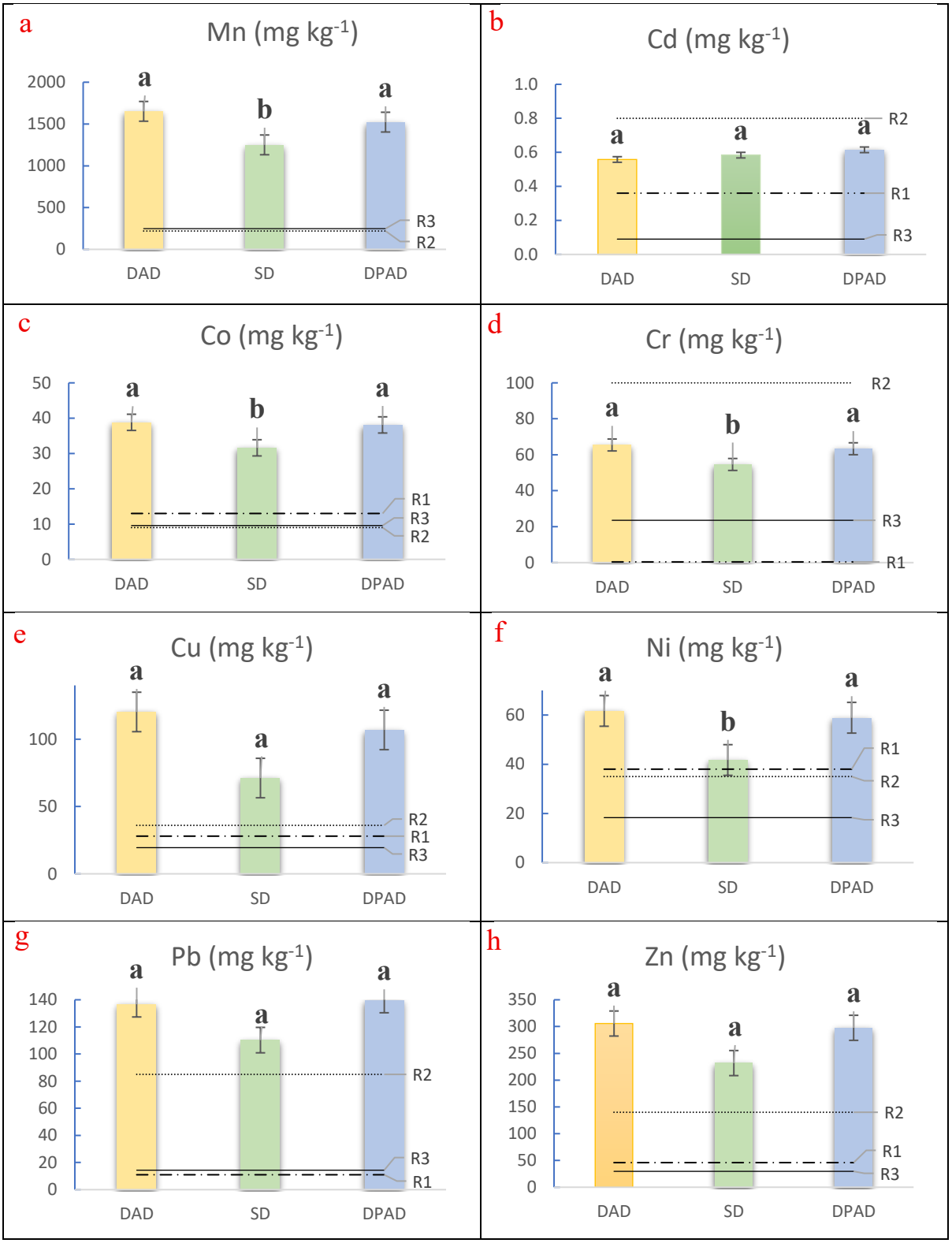
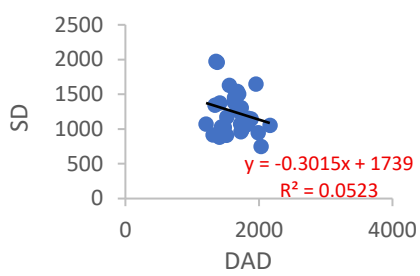
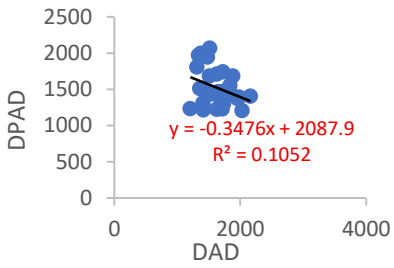

a
Mn (mg kg-1)
2000
1500
1000
500
0
a
b
a
R3
R2
DAD
SD
DPAD
b
Cd (mg kg-1)
1.0
0.8
0.6
0.4
0.2
0.0
a
a
a
R2
R1
R3
DAD
SD
DPAD
c
Co (mg kg-1)
50
40
30
20
10
0
a
b
a
R1
R3
R2
DAD
SD
DPAD
d
Cr (mg kg-1)
100
80
60
40
20
0
a
b
a
R2
R3
R1
DAD
SD
DPAD
e
Cu (mg kg-1)
100
50
0
a
a
a
R2
R1
R3
DAD
SD
DPAD
f
Ni (mg kg-1)
60
40
20
0
a
b
a
R1
R2
R3
DAD
SD
DPAD
g
Pb (mg kg-1)
140
120
100
80
60
40
20
0
a
a
a
R2
R3
R1
DAD
SD
DPAD
h
Zn (mg kg-1)
350
300
250
200
150
100
50
0
a
a
a
R2
R1
R3
DAD
SD
DPAD

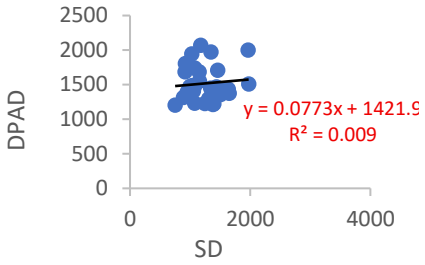
Fig. 3

1137

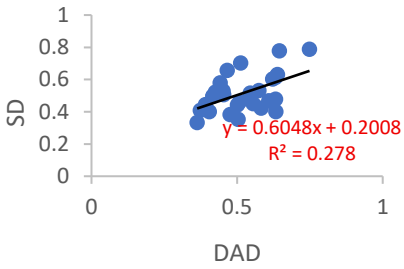
a. Mn

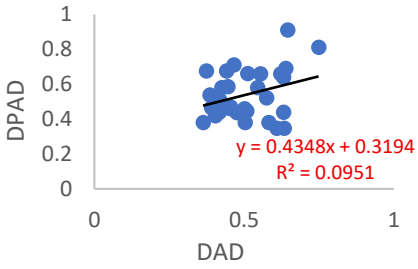


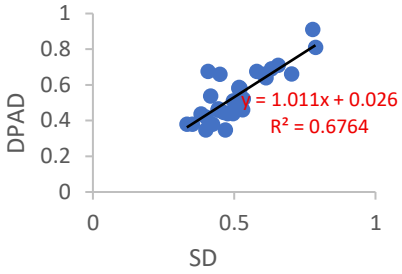




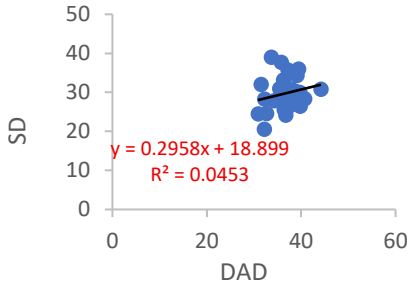
b. Cd

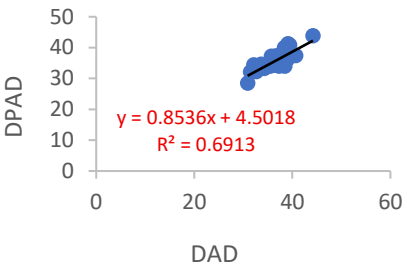


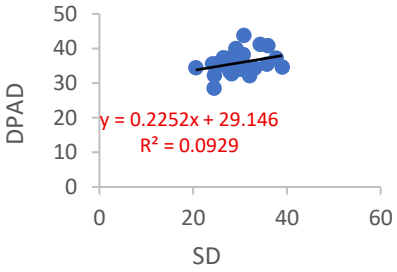




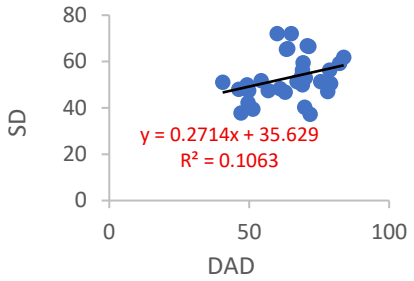
c. Co

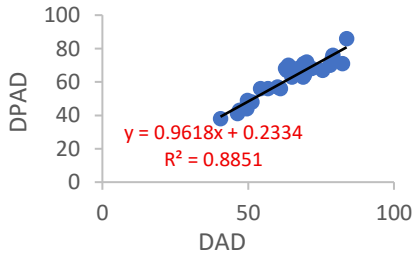


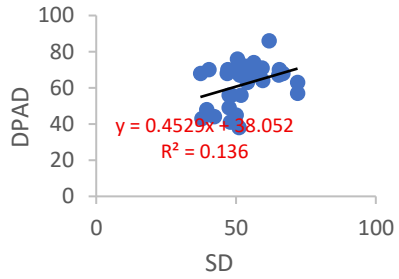




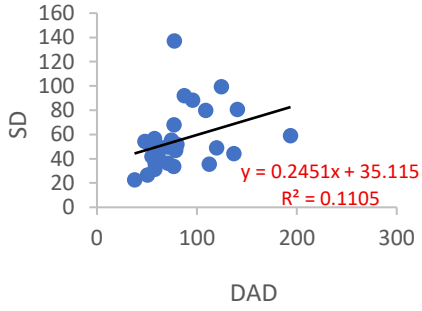
d. Cr

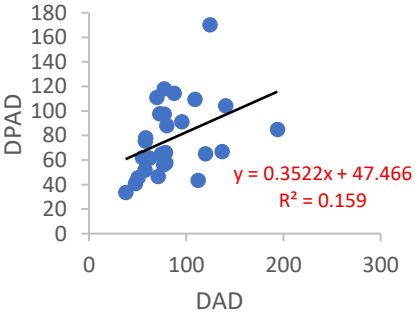


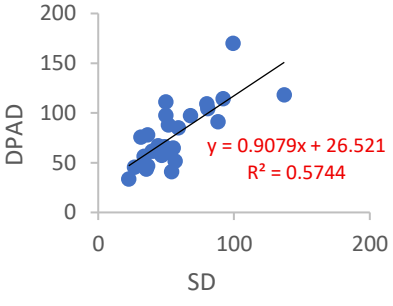




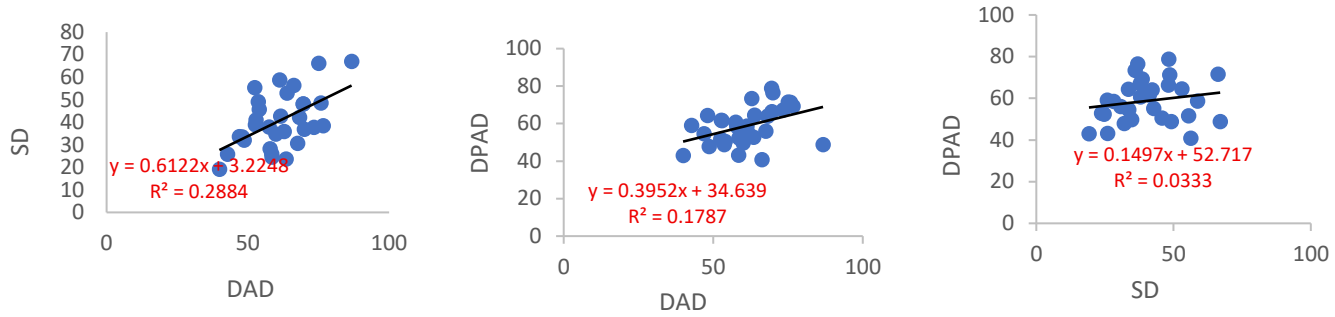
e. Cu



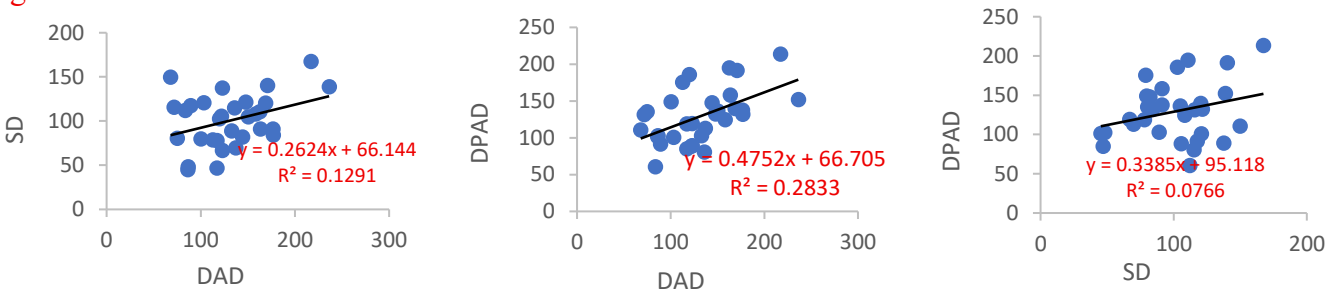




f. Ni



g. Pb



h. Zn

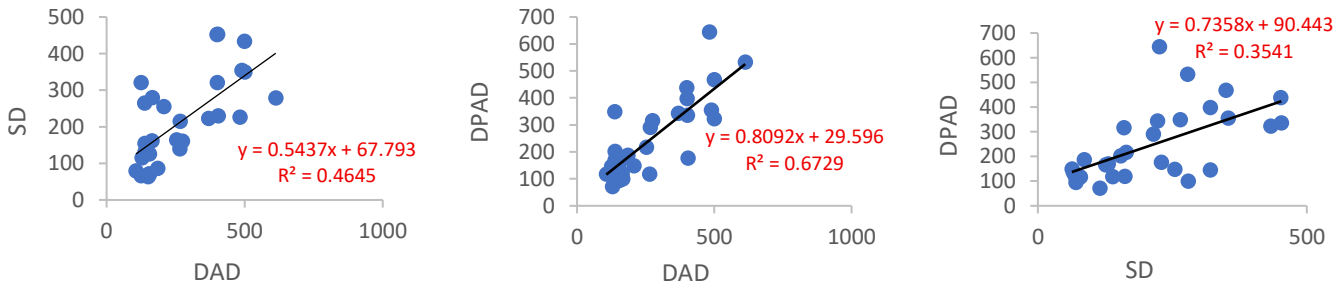


Fig. 4

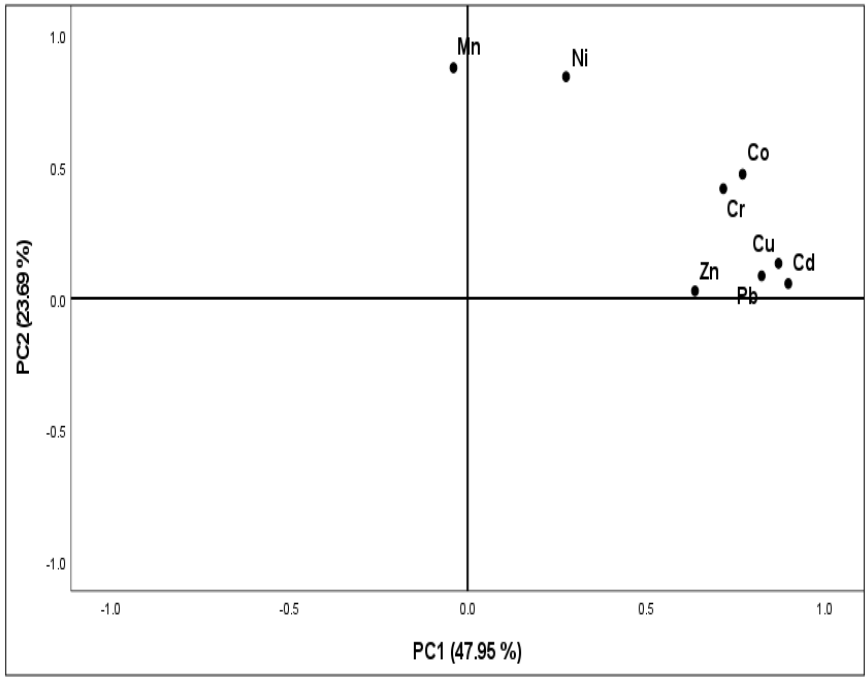

Mn
Ni
Co
Cr
Cu
Cd
Zn
Pb
1.0
0.5
0.0
-0.5
-1.0
PC2 (23.69 %)
PC1 (47.95 %)

Fig. 5

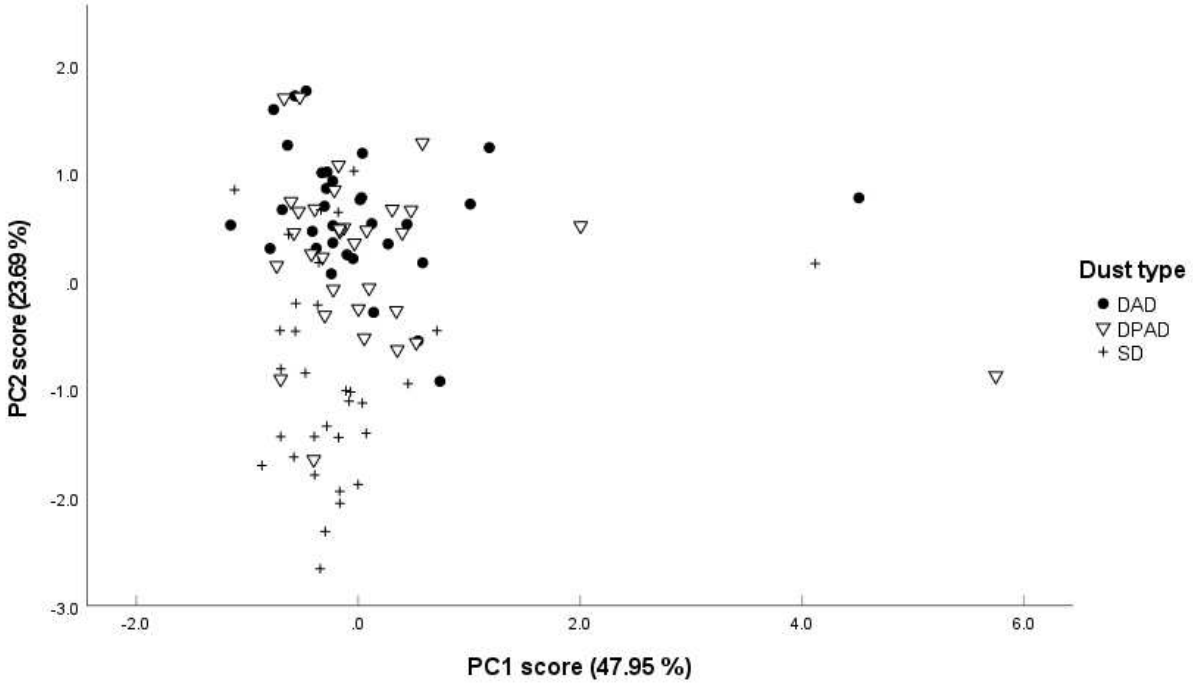

2.0
1.0
.0
-1.0
-2.0
-3.0
PC2 score (23.69 %)
-2.0
.0
2.0
4.0
6.0
PC1 score (47.95 %)
Dust type
DAD
DPAD
SD

Fig. 6

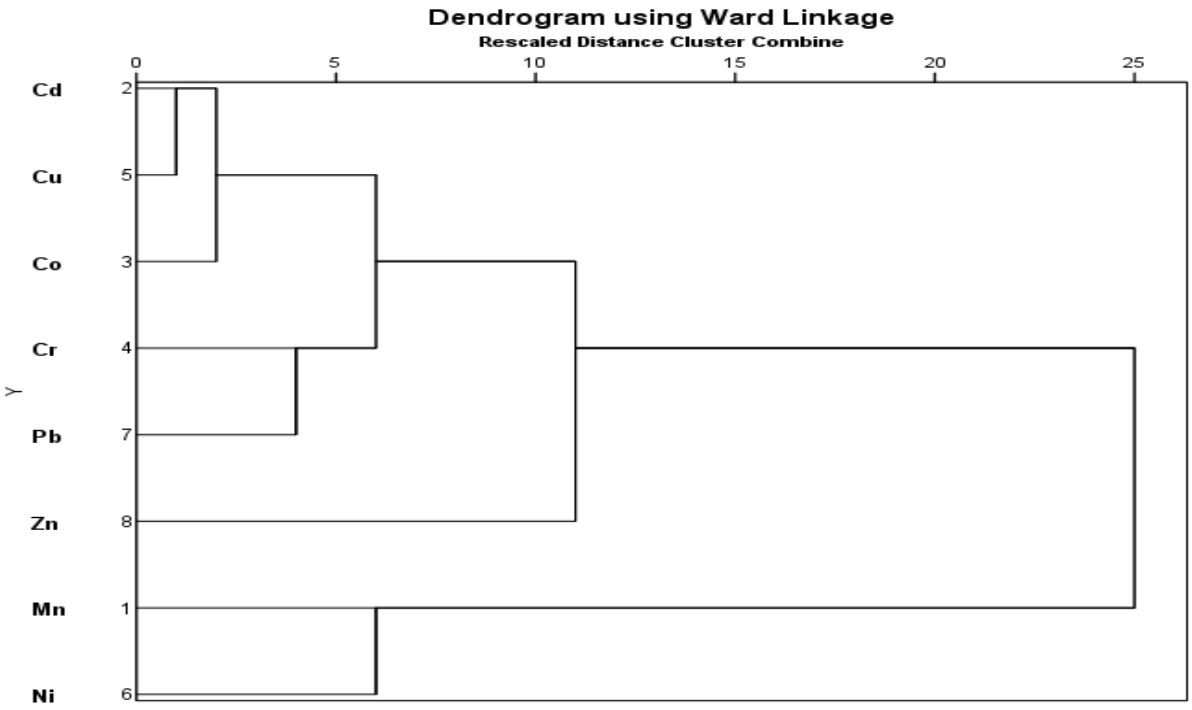

Dendrogram using Ward Linkage
Rescaled Distance Cluster Combine
0
5
10
15
20
25
Cd
Cu
Co
Cr
Pb
Zn
Mn
Ni
2
5
3
4
7
8
1
6
Y

Fig. 7

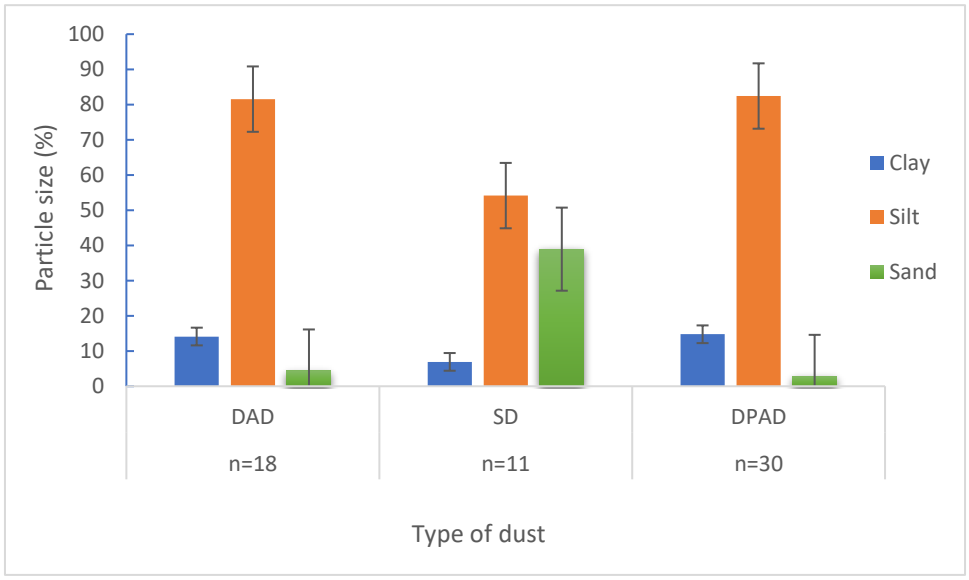
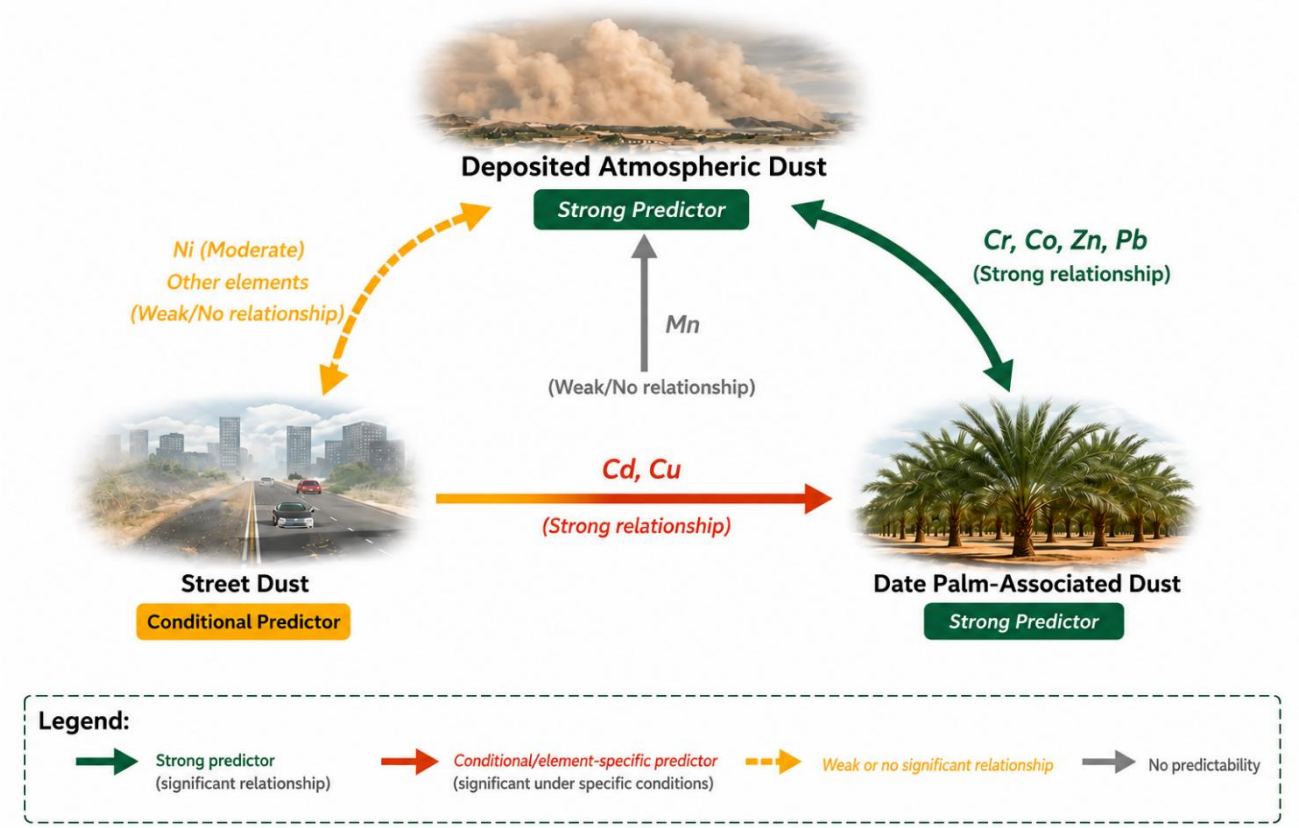

Particle size (%)
100
90
80
70
60
50
40
30
20
10
0
Clay
Silt
Sand
DAD
n=18
SD
n=11
DPAD
n=30
Type of dust

Fig. 8

.



1

1168 **Fig. 9**

1169

1170

1171

1172

1173

1174

Supplementary Files

This is a list of supplementary files associated with this preprint. Click to download.

- Highlights.docx